Review of Computational Fluid Dynamics in the Design of Floating Offshore Wind Turbines

Rizwan Haider [1,2], Xin Li [1,2,3,*], Wei Shi [2], Zaibin Lin [4], Qing Xiao [5] and Haisheng Zhao [1,2]

1   School of Hydraulic Engineering, Faculty of Infrastructure Engineering, Dalian University of Technology, Dalian 116024, China; rizwanhaider@mail.dlut.edu.cn (R.H.); hzhao@dlut.edu.cn (H.Z.)
2   State Key Laboratory of Coastal and Offshore Engineering, Dalian University of Technology, Dalian 116024, China; weishi@dlut.edu.cn
3   Ningbo Institute of Dalian University of Technology, Ningbo 315032, China
4   School of Engineering, University of Aberdeen, Aberdeen AB24 3UE, UK; z.lin@abdn.ac.uk
5   Department of Naval Architecture, Ocean and Marine Engineering, University of Strathclyde, Glasgow G4 0LZ, UK; qing.xiao@strath.ac.uk
*   Correspondence: lixin@dlut.edu.cn

Abstract: The growing interest in renewable energy solutions for sustainable development has significantly advanced the design and analysis of floating offshore wind turbines (FOWTs). Modeling FOWTs presents challenges due to the considerable coupling between the turbine's aerodynamics and the floating platform's hydrodynamics. This review paper highlights the critical role of computational fluid dynamics (CFD) in enhancing the design and performance evaluation of FOWTs. It thoroughly evaluates various CFD approaches, including uncoupled, partially coupled, and fully coupled models, to address the intricate interactions between aerodynamics, hydrodynamics, and structural dynamics within FOWTs. Additionally, this paper reviews a range of software tools for FOWT numerical analysis. The research emphasizes the need to focus on the coupled aero-hydro-elastic models of FOWTs, especially in response to expanding rotor diameters. Further research should focus on developing nonlinear eddy viscosity models, refining grid techniques, and enhancing simulations for realistic sea states and wake interactions in floating wind farms. The research aims to familiarize new researchers with essential aspects of CFD simulations for FOWTs and to provide recommendations for addressing challenges.

Keywords: computational fluid dynamics; floating offshore wind turbines; uncoupled CFD models; partially coupled CFD models; fully coupled CFD models

1. Introduction

The increase in global population and industrial activities has driven up energy demand [1]. The rapid depletion of fossil fuels and other non-renewable resources has shifted attention toward renewable energy, seen as a source of sustainable and affordable power [2]. Recently, the focus on developing and utilizing offshore wind energy has intensified, leading to substantial improvements in the designs, construction, operations, and maintenance of offshore wind turbines. Offshore wind energy, compared to its onshore counterpart, offers clear advantages such as consistently higher wind speeds, reduced turbulence, more available space, and no visual or noise pollution [3].

Wind turbines located offshore are categorized into two types: bottom-fixed turbines and FOWTs. The base of the bottom-fixed turbines is embedded into the ocean floor, whereas FOWTs utilize buoyant support structures that are linked to the seabed by mooring lines [4]. For bottom-fixed turbines, a key limitation is that they are suited only for water depths up to 60 m. If the depth exceeds 60 m, known as deep water, the expense associated with constructing and mounting their foundations escalates sharply, rendering them economically impractical for commercial use [5]. Interestingly, more than 80% of wind

resources are found in areas where the water depth is more than 60 m. To economically exploit these deep-sea wind resources, FOWTs have been crafted and refined. Notably, the mooring system of FOWTs contributes significantly to costs, with mooring line lengths typically quadrupling the water depth. Additionally, the technology supporting FOWTs is less developed when compared to bottom-fixed turbines, resulting in higher levelized costs of energy (LCOEs), which currently hinders their widespread commercial adoption [6]. Projections indicate that the LCOE for bottom-fixed turbines will see a reduction of 70% from the levels in 2015 by the year 2025, with FOWTs expected to follow a similar cost reduction trajectory by 2030 [7].

FOWTs, due to rotation axis, are further categorized into two main types, namely, vertical axis wind turbines (VAWTs) and horizontal axis wind turbines (HAWTs). The blades of the turbines in HAWTs rotate around the horizontal axis, which means they are parallel to the direction of the wind. On the other hand, the blades of the turbines in VAWTs rotate around the vertical axis, positioning them perpendicular to the wind direction. In terms of construction, a heavy generator is positioned at the top of the tower in HAWTs, whereas, for VAWTs, the generator is located at the bottom. HAWTs necessitate a yaw control mechanism to adjust the rotor's orientation in alignment with the wind direction. VAWTs, conversely, have the capacity to produce energy from winds arriving from all directions. A significant limitation of VAWTs is their reduced effectiveness in energy production compared to HAWTs [8]. Owing to their superior performance, most floating offshore structures worldwide prefer HAWT technology. For a more thorough examination of VAWTs, references [9–11] in the literature offer extensive discussions. Nevertheless, the central theme of this paper is dedicated to examining HAWTs.

In the upcoming years, FOWTs are anticipated to surpass bottom-fixed turbines regarding cost-effectiveness for commercial usage, driven by substantial advancements in technology. Nonetheless, the design process for FOWTs still requires intensive attention and additional effort in several crucial areas. One significant concern remains the vigorous interaction among the turbine and its buoyant base. Different from their bottom-fixed counterparts, FOWTs display pronounced unsteady aerodynamic behaviors caused by the movements of the floating structures, which are influenced by ocean waves and current [12]. Furthermore, the motion dynamics of these platforms are heavily impacted by the aerodynamic forces that act on the turbine blades and are then conveyed through the structure of the tower. Beyond the dynamics between hydrodynamics and aerodynamics in FOWTs, an additional major consideration remains the aeroelastic effects that arise from increasing the diameter of the rotor blades. Although the initial LCOE for FOWTs remains higher than that for onshore turbines, technological progress in the rated power of offshore turbines is expected to lead to a reduction in costs by approximately 8.5%, surpassing the benefits seen in improvements to aerodynamics and the design and setup of floating platforms [13]. This shift towards larger FOWTs is aimed at making them more economically viable in commercial markets, thus highlighting the significance of the aeroelastic responses of the blades. Moreover, issues such as fatigue loads and the potential for structural failures in turbine blades are increasingly critical, especially under extreme marine conditions. Therefore, with FOWTs moving towards larger sizes and deeper offshore implementations, there is a pressing need for more comprehensive and detailed studies on their fully integrated aero-hydro-elastic performance to enhance their dependability in varied wind and wave conditions.

Research on FOWTs is divided into three distinct segments: prototyping, scaled-down experimental studies, and numerical simulations, each of which is extensively reviewed in the academic literature [14–19]. Advances in high-performance computing (HPC) have significantly enhanced the scope and focus on numerical simulations for FOWTs. Various specialized codes have been formulated for this purpose [20]. Notably, the use of the blade element momentum (BEM) approach [21] and potential flow (PF) techniques [22] are prevalent in the preliminary stages of FOWT design. However, these economical models, while saving computational resources, fall short in capturing viscous phenomena, which are crucial for the accurate prediction of aerodynamics associated with turbine blades,

towers, and hubs, as well as the hydrodynamics of floating platforms. To address these limitations, additional corrective models are often required to refine BEM outputs to ensure accuracy [23]. The capability of BEM to predict aerodynamic loads accurately warrants further comprehensive study, especially given the complex inflow conditions associated with FOWTs from platform movements. Moreover, the capacity of potential-based techniques in capturing the intricate flow dynamics and nonlinear behaviors is limited, as they cannot effectively represent flow separation around the platforms. By contrast, the application of high-fidelity CFD can overcome these drawbacks [24]. Although initially costly, the computational expense of CFD is expected to decrease, becoming more economically viable, as a result of the continued progress in HPC technologies. Hence, this study prioritizes the application of high-fidelity CFD techniques in the ongoing development and refinement of FOWT design strategies.

FOWTs represent a critical focus of contemporary research, with a substantial body of literature examining their hydrodynamic and aerodynamic characteristics [8,25–30]. Our review uniquely addresses the comprehensive application of CFD in the design and analysis of FOWTs, focusing extensively on the spectrum from uncoupled to fully coupled modeling techniques. This detailed focus on CFD differentiates our work from Subbulakshmi et al. [8], who review broader experimental and numerical methods, and from Wang et al. [17], who concentrate on aerodynamic interactions and platform dynamics. While Edwards et al. [29] provide a historical perspective on FOWT platform designs, our review explores the advanced CFD techniques that are crucial for the next generation of FOWT design. Moreover, although Ojo et al. [31] discuss the optimization frameworks within FOWT substructures, our review specifically identifies the integration of CFD within these frameworks to enhance design accuracy and efficiency. Similar to Xu et al. [32] and Zhang et al. [33], our paper highlights the importance of high-fidelity CFD simulations; however, we advance the discussion by proposing specific improvements, such as nonlinear eddy viscosity models and enhanced grid techniques, which are crucial for addressing the complex dynamics of FOWTs. Our review thereby not only fills a critical gap in detailing CFD's role in advancing FOWT technology but also sets forth a clear direction for future research, offering substantial contributions to both the academic and practical aspects of renewable energy development.

The remainder of this paper is organized into several key sections: Section 2, "Mechanisms and Dynamics of FOWTs", provides a detailed discussion on the various components and dynamic interactions within FOWTs. Section 3, "Numerical Modeling", presents methodologies for simulating FOWTs, discussing uncoupled to fully coupled analysis techniques, and, also, the implications for design and analysis accuracy. Section 4 "CFD Modelling for FOWTs Analysis", explores the specific application of CFD in enhancing the understanding of aerodynamic and hydrodynamic behaviors critical to FOWT performance. Section 5, "Challenges and Recommendations", outlines existing research gaps and methodological limitations, and proposes strategic directions for advancing the field. The paper concludes in Section 6, "Conclusion", summarizing the findings, emphasizing the importance of CFD in the design of FOWTs, and suggesting future research directions to improve their effectiveness and efficiency.

2. Mechanisms and Dynamics of FOWTs

2.1. Overview

The FOWT is composed of multiple components, which include the wind turbine itself (featuring the rotor, nacelle, and tower for electricity generation), a floating platform that supports the turbine, and an anchoring system designed to stabilize the platform's position, as depicted in Figure 1. Differing from fixed offshore turbines, FOWTs experience continuous motion because they operate in complex environmental conditions. The dynamic movements of the floating structure are influenced not only by the direct impact of the wave and current loadings on the platform but also by wind forces impacting the turbine, affecting the comprehensive system load and the resultant dynamic responses. Moreover,

the system's six DOF movements comprising translational movements (surge, sway, and heave) and rotational movements (roll, pitch, and yaw) alter the turbine's position and orientation. These changes affect the relative speed of the wind encountered by the turbine blades, thereby impacting the aerodynamic performance and energy production capabilities. The integration of the anchoring system adds another layer of complexity, as the platform is both constrained and supported by the anchoring forces, which are themselves dependent on the platform's kinetic behavior. Figure 2 illustrates the interactions among the various FOWT components. Therefore, it is crucial to consider these interconnected effects during the design phase of an FOWT to ensure optimal performance and stability.
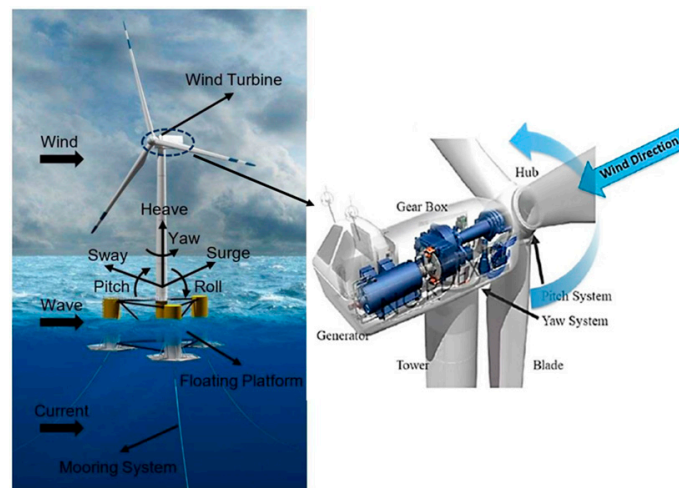

Figure 1. FOWT components [34,35].
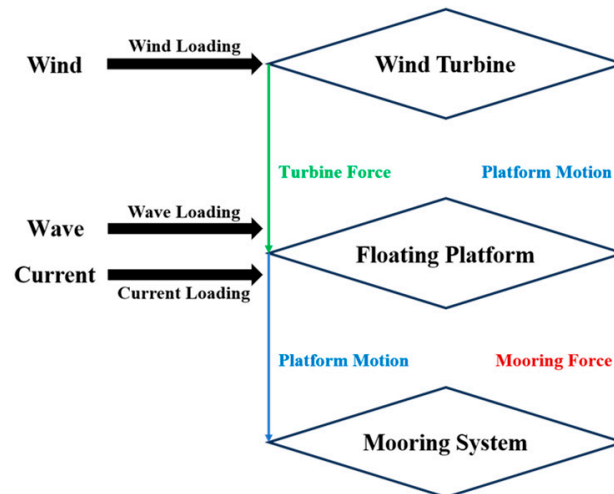
Figure 2. Coupling of FOWTs.

FOWTs are categorized by their support structures, with several common types showcased in Figure 3. In areas where the water is shallow, offshore wind turbines typically utilize fixed supports such as monopiles or jackets. Yet, as the depth exceeds 50 m, these fixed supports prove to be neither reliable nor cost-effective, prompting the development of floating platforms. The significant benefits of FOWTs in deeper water include more consistent wind conditions and a reduction in environmental disturbances; they generate less noise and are virtually unseen from the shore [31]. Furthermore, specific floating platform designs can be constructed at a port and then towed to their operational locations, streamlining both installation and ongoing maintenance. With these advantages, FOWTs are expected to gain a competitive edge in future energy markets.

Figure 3. Types of FOWT platforms [35].

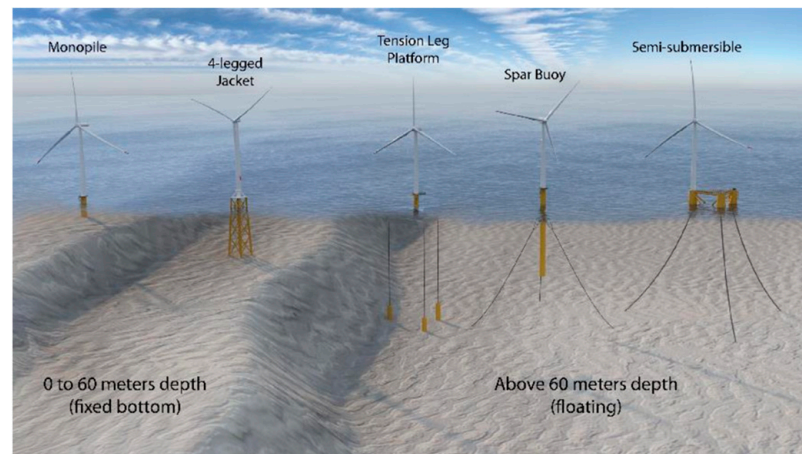*2.2. FOWT Assembly and Control System*

Major structural elements of a wind turbine include the assembly (tower and the rotor-nacelle, with the latter comprising blades, a drivetrain, the nacelle, and the hub). The effective modeling of these components is crucial in order to accurately assess structural deformations, which directly impact the loads from wind and waves that the FOWTs must withstand. Commonly, flexible elements like towers and rotor blades are depicted through a linear modal framework [36]. Mode shapes for these components are established through eigenvalue calculations, and, typically, only the primary modes are utilized in the analysis. The drivetrain's dynamics are captured with a sole torsional mode. The nacelle and hub, on the other hand, are considered rigid bodies connected through flexible connections. The approach called lumped mass, incorporating linear stiffness and damping, is applied to model rigid elements [37]. These methods, while straightforward, are suited primarily for small-scale deformations. A more advanced method involves employing flexible–rigid multibody simulations that incorporate various complexities to better understand the interactions between the FOWT's different structural modes [38]. This approach, however, tends to require a greater number of computational resources and time.

FOWTs are equipped with sophisticated control systems that include a range of sensors and actuators. The controller's main function is to process data from these sensors and send appropriate commands to the actuators. This enables optimal power extraction from the wind while maintaining the turbine's safe operation, mitigating loads, and preventing malfunctions. The operational modes of the turbine are categorized in different regions, according to wind velocity, each with specific control objectives, depicted in Figure 4. Region 1 is characterized by wind speeds that are too low to activate the turbine, keeping it in an idle state without generating power. In Region 2, which extends from the initiation to the maximum wind velocities, the power output rises with increasing wind speed. Achieving maximum power in this area may involve adjusting the rotor's angular velocity [39,40] or the torque [41], as discussed in detail by Kumar and Chaterjee [42]. The transition zone between regions 2 and 3 uses fixed blade pitch angles and closed-loop torque management to maintain a steady rotor speed. Region 3 covers wind speeds from the maximum to the cessation limits, where the output is maintained steady at the maximum power. Therefore, in this zone, controllers of blade pitch [43,44] modify the pitch to keep the power output stable, helping control the generator's speed and minimizing mechanical strain on the structure. Region 4 involves shutting down the turbine using mechanical brakes to protect against damage from severe wind gusts. Additional structural stability is provided by apparatuses like tuned mass dampers [45–48], tuned liquid dampers [49], and damping elements [50,51]. Each of these control strategies and their purposes are systematically outlined in Table 1, showcasing the different operational approaches used in FOWT management.
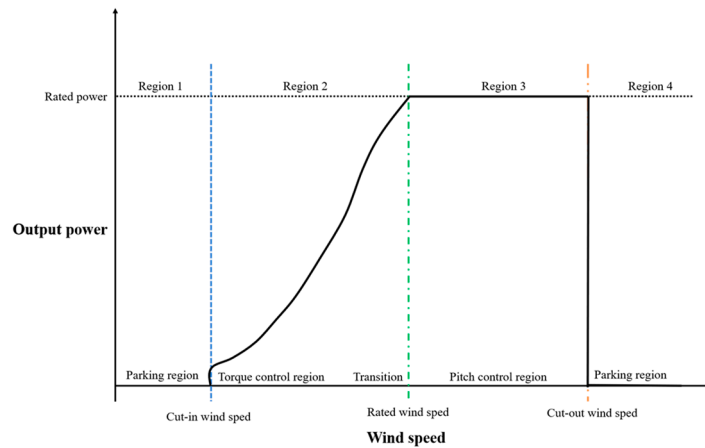
Figure 4. Wind turbines: operational regions and control objectives. Reproduced with permission from [8], Elsevier, 2022.

Table 1. FOWT control system. Reproduced with permission from [8], Elsevier, 2022.

Controller		Objective
Blade-pitch controller		Maximize the output power
Vibration controller		Maintain generator output at the rated power
Generator torque controller		Minimize structural vibrations

Standard control methods are generally appropriate for systems that function with one input and one output. However, considering multi-input multi-output (MIMO) configurations for FOWTs could significantly enhance their efficiency. In pursuit of this, several sophisticated control approaches tailored to MIMO configurations have been implemented in FOWT applications. Among these progressive methods are the linear quadratic regulator [52], sliding mode control [53], linear parameter varying control [54], model predictive control [55], and H-infinity control [56]. These approaches generally depend on a simplified model of the system, and the presence of unmodeled dynamics might impair the overall system performance. Presently, there is an increasing exploration of data-driven control methods, which influence the actual input–output data from the system to formulate control designs. This area of study is looking into various machine-learning techniques, such as genetic algorithms, reinforcement learning, and bio-inspired methods, to develop optimal control strategies for FOWTs [57]. These modern techniques are being examined for their potential to enhance control precision by utilizing real-time data, thus allowing for adaptive responses to changes within the system.

2.3. FOWT Floating Platform Types

A standard design does not exist for floating platforms; instead, four main types are recognized, each tailored for optimal performance in particular environmental conditions due to distinct advantages and limitations. These types are semi-submersibles, barges,

tension-leg platforms (TLPs), and spar buoys, showcased in Figure 5. Detailed information on each platform type is provided in the sections that follow. Additionally, these platforms are categorized based on their stability mechanisms, which are illustrated in Figure 6. A comprehensive overview is provided in Table 2.
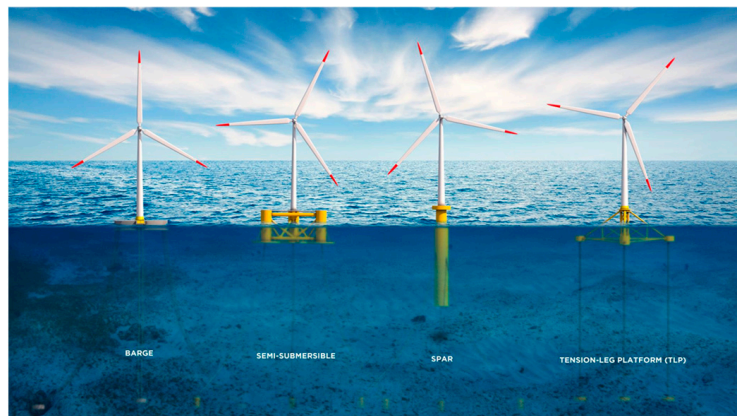

Figure 5. Platform types [58].

Table 2. Design concept comparisons.

	Semi & Barge	TLP	Spar
Mooring Lines	3–5	5–7	3–4
Water Depth (m)	50–300	50–350	100–400
Footprint	Large	small	Large
Seabed Condition	Unlimited	Limited	Unlimited
Assembly	Port-side	Port-side	Offshore
Capital Expenditures	Low	Medium	High

2.3.1. Spar Buoy

The floating platforms called spar buoys employ substantial cylindrical forms, stabilized with ballast and secured using catenary mooring systems. Typically constructed from steel or concrete, these cylinders are ballasted with water and soil to ensure the substructure's lower half is heavier, while the upper half, closer to the surface, remains lighter and has a large draft. The key benefit of the design of spar buoys is the simplicity and superior solidity, facilitating easier standardization and normalization. However, the significant size of these structures tends to increase the overall cost of the platform. Moreover, the necessity for a substantial draft indicates that these platforms must be positioned in deeper marine environments [59].

2.3.2. Tension-Leg Platform (TLP)

The TLP utilizes a submerged buoyant structure securely fastened to the seabed using a taut-leg mooring setup known as vertical tendons, constructed from steel to enhance the platform's buoyancy and stability. The primary benefit of this platform type is its relatively smaller and lighter substructure, which translates to lower material expenses. The taut-leg system creates vertical tension at the anchoring points and requires a smaller area due to its compact footprint. Anchor solutions such as gravity anchors, suction anchors, or anchor piles are selected based on the seabed's condition and geological characteristics to handle significant vertical forces. However, should the tendons fail, there is a risk of the platform capsizing. Stability issues are prominent with the TLP prior to anchorage, and it is challenging to disconnect once deployed. Moreover, if wind turbines are assembled and serviced onshore or in a dry dock, considerations for their transportation to the site become crucial. These aspects increase operational risks and add complexity to the construction process [60].

2.3.3. Semi-Submersible

The semi-submersible floating platform combines two distinct design approaches. It employs a distributed buoyancy-stabilized system and uses a catenary mooring system to connect to the sea floor, ensuring stability. This type of platform has a shallower draft compared to the spar-buoy platform, typically less than 10 m. This allows for deployment in waters with depths of about 40–50 m [59]. Additionally, the reduced draft enables the wind turbine systems to be installed at harbor facilities and then transported offshore using tug boats. A key benefit of semi-submersible platforms is their adaptability to various water depths, utilizing internal ballast for stabilization adjustments. Regarding operation and maintenance (O&M), this structure considerably reduces the requirement for employees and machinery [59].

2.3.4. Barge-Type

The design of the barge floating platform is an expanded version of the semi-submersible model. This platform comprises either a concrete or steel hull that maintains buoyancy with a shallow draft, specifically structured to sustain wind turbine systems. It employs a distributed buoyancy-stabilization approach, utilizing a broad, weighted water plane area for stability. The barge's layout features either a square or ring-like shape with a central area known as the moon pool, which mitigates wave-induced movements by absorbing wave loads. Due to its geometrical design, the extensive surface area of the platform is well-suited to accommodating transmission equipment. The design also facilitates straightforward maintenance and repair activities [61].
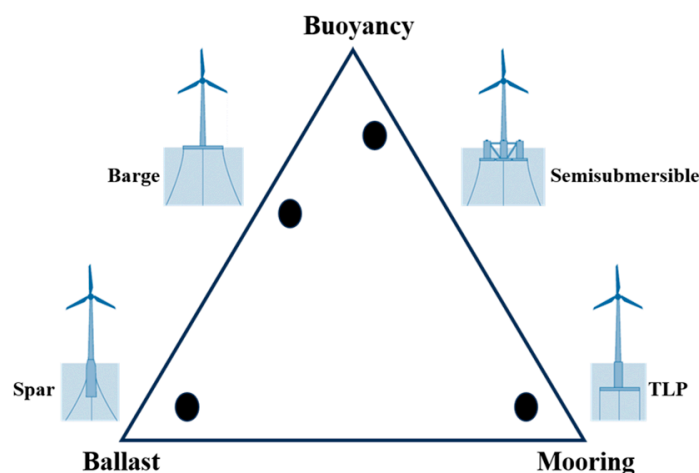

Figure 6. FOWT platform stability triangle [62].

2.4. Mooring Lines

Mooring lines are essential for stabilizing floating platforms in the ocean, helping to secure their position and provide stability against environmental loads. These lines fall into two primary categories: taut and catenary mooring. FOWTs typically utilize a multi-point mooring setup, incorporating numerous attachment points for the mooring cables. Recently, single-point mooring (SPM) configurations, which connect mooring cables at a single attachment point, have been implemented for FOWTs [63]. A novel SPM system proposed by Nihei et al. [64] functions as a weathervane, allowing a floating structure with a downwind rotor to rotate unrestricted, thereby eliminating the need for a yaw control system. The dynamic behavior of mooring lines is depicted through various models of differing complexity. These models and their features are illustrated in Figures 7 and 8. Figure 7 details the quasi-static mooring model, considering seabed interaction and line elasticity. Figure 8 describes dynamic models that incorporate additional factors such as seabed interaction, line elasticity, bending stiffness, inertia, and damping. Further details about these models are explored in the sections that follow.
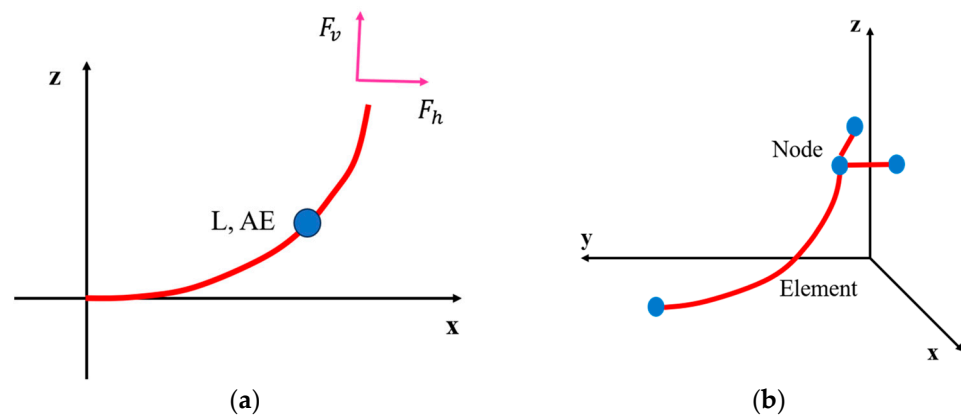
Figure 7. Quasi-static mooring model: (**a**) single line element, and (**b**) multi-segment line element.
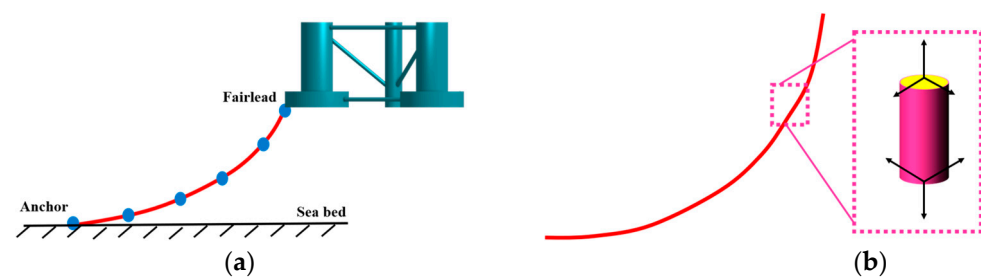

Figure 8. Dynamic mooring models: (**a**) lumped mass, and (**b**) finite element.

2.4.1. Quasi-Static Approach

These frameworks calculate the tension analytically in the mooring cables and operate under a quasi-static framework, treating each mooring cable as a singular linear element [65]. They integrate effects such as buoyancy, line elasticity, and seabed friction. However, these frameworks omit considerations of inertia, hydrodynamics, and damping effects on the mooring cables. One significant limitation of these frameworks is that they only provide restoring forces constrained to the plane aligned with the mooring cable. To address this restriction, Masciola et al. [66] developed a method using multi-segment line elements for the mooring cables, which allows for assessing the restoring forces in multiple directions, thus enhancing their suitability for practical anchoring configurations.

2.4.2. Lumped Mass Approach

In modeling, mooring cables are considered as multibody elements that are connected by dampers and springs [67]. The interaction between the mooring cable and the seabed is represented through a Coulomb friction element. To calculate the restoring forces exerted by the mooring cables, a series of differential equations that ensure dynamic equilibrium and continuity at each multibody system node are formulated and resolved. One limitation of the lumped mass frameworks is their lack of consideration for the torsional stiffness in mooring cables. However, the benefit of using lumped mass frameworks lies in their utilization of the same mathematical approach for representing the equilibrium of the structural dynamic, which is similarly employed in modeling turbine towers. This uniformity allows for a single module to simulate both the towers and the mooring cables effectively. The simplicity of these frameworks has led to their widespread adoption among researchers [12].

2.4.3. Finite Element Modeling Approach

Hydrodynamic and inertia effects, which are neglected by the quasi-static approach, can impose additional forces on mooring cables. Situations such as snap loading caused by mooring cable failure necessitate the use of dynamic models for proper evaluation. Adopting finite element methods (FEMs) allows for a more sophisticated approach to

accurately simulating mooring cable behavior in these instances. FEM models are capable of incorporating both torsional and bending stiffness into the mooring line calculations. Although utilizing finite elements for the detailed discretization of mooring lines enhances model accuracy, it also significantly increases computational time and costs. Numerous studies have examined the critical role of the dynamic modeling of mooring lines, particularly their responsiveness across various water depths. Ishihara et al. [68] evaluated a semi-submersible platform's behavior using both a linear spring-damper model and an FEM model of mooring lines alongside experimental data, pinpointing the deficiencies of linear approaches. Hall et al. [69] explored how mooring line fidelity affects FOWT response, discovering that quasi-static models could lead to a 30% error in assessing damage-equivalent and extreme loads during significant platform movements. Azcona et al. [70] developed software that utilizes an FEM model for mooring lines, which accounts for axial elasticity, nonlinear hydrodynamics, and interactions with the seabed. Due to their intensive computational demand, these models are generally recommended for use only in the latter stages of design. In addition to these, the MooDy FEM mooring code, which is based on a discontinuous Galerkin FEM formulation [71], has been applied in the coupled mooring analysis for floating wave energy converters (WECs) using CFD. This approach enables the detailed and accurate modeling of the dynamic interactions between the mooring lines and the floating structures, improving the reliability of the simulations for WEC applications [72].

2.5. Anchoring System

The selection of an anchoring system is influenced by the type of mooring system in use, the necessary anchoring capacity, and the seabed conditions. Drag-embedded anchors typically support catenary mooring lines. For taut mooring lines, which are subjected to substantial vertical loads, the preferred choices are gravity or drive/suction piles anchors. The anchoring system's capacity is determined by the sizes of the anchor as well as the condition of the seabed. Notably, the anchoring strength in sand and hard clay surpasses that in soft clay. Detailed information on various anchoring systems is documented in the reference [73]. The different anchoring systems applicable to FOWTs are outlined in Table 3.

Table 3. FOWT anchoring systems. Reproduced with permission from [8], Elsevier, 2022.

Anchors		Properties
Gravity anchor		Installation and retrieval are easy Capacity is governed primarily by soil type and weight
Drag anchor		Installation is fast Capacity depends on soil type, and penetration depth achieved Retrievable
Suction anchor		Not suitable for very stiff clay/thick sandy stratum Capacity is governed by suction anchor size Installation is aided by underwater remotely operating vehicle Retrievable
Driven pile		Pile drivability analysis is required to ensure the capacity Installation is aided by hammer Recovery is difficult

3. Numerical Modeling

3.1. Background

For numerical modeling purposes, the FOWT is typically analyzed across three interrelated domains: hydrodynamics, structural dynamics, and aerodynamics, as shown in Figure 9. These domains are modeled using various approaches (uncoupled, partially cou-

pled, and fully coupled), different levels of fidelity (low, medium, and high), and software. An explanation is provided in the following sections.
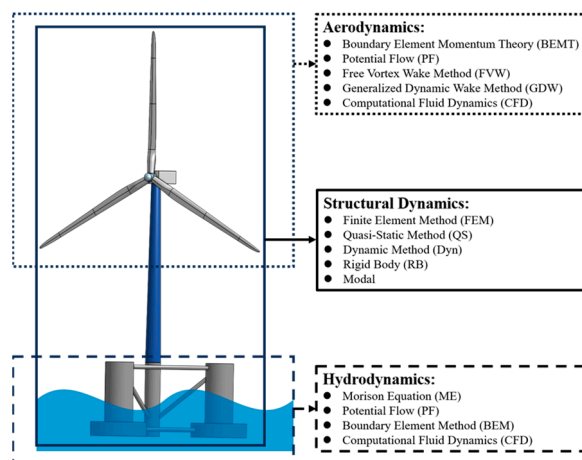

Figure 9. FOWT numerical structure.

3.1.1. Analysis Approaches

(A) Uncoupled: FOWTs face the dynamic environmental forces of wind and waves. To thoroughly understand the global structural behavior of FOWTs, it is important to consider the simultaneous impacts of the forces of wave and wind using an integrated analysis approach. Yet, incorporating the movement of both the turbine and the floating structure adds complexity to the experimental setups and numerical models. The capability to perform these complex experiments is often limited by the existing facilities, both in terms of computing and practical experiment resources. To avoid these limitations, an uncoupled analysis method is utilized for FOWTs. This method simplifies the process by analyzing the effects of wave and wind conditions separately rather than together. For instance, the hydrodynamic behavior might be studied by subjecting the floating structure with a turbine model to wave conditions only, either in a wave-testing facility or through targeted numerical models. Similarly, the aerodynamic behavior can be analyzed by testing a scaled model of the turbine in an aerodynamic testing facility or through models that specifically exclude wave and floating structure effects.

(B) Partially coupled: In the analysis of a partially coupled approach, both aerodynamic and hydrodynamic factors are considered, although one is typically streamlined to enhance the examination of the other. For instance, when evaluating the hydrodynamic behavior of a floating structure equipped with a turbine, the aerodynamic elements are estimated. Conversely, when the emphasis is on aerodynamics, the motion of the floating structure is simulated in a systematic way using an induced oscillation technique. This method effectively simplifies the analysis. Employing this technique, the overall behavior of the FOWTs facing combined wave and wind forces can be assessed, either via scale-model experiments in a wave-testing facility or through numerical simulations conducted under partially coupled conditions. In these tests, the floating structure with a turbine model is exposed to both wave and wind impacts, although with some wind load estimates. Likewise, the response of the floating structure to wave influences can be replicated as induced oscillations in specific DOF on a scaled turbine model within an aerodynamic testing facility.

(C) Fully coupled: The analysis of partially and uncoupled FOWTs do not entirely capture the intricate interactions involving the movement of the floating platform and wind turbine, as these methods tend to approximate either the aerodynamic or hydrodynamic aspects. Therefore, to accurately assess the true behavior of FOWTs under simultaneous wave and wind forces, a completely coupled analysis is essential. This comprehensive analysis typically involves numerical simulations, which can be conducted through CFD or via other simulation tools such as HAWC2 [74], FAST [75], and Bladed [76]. In exper-

imental settings, hybrid methods are employed to effectively merge aerodynamic and hydrodynamic studies.

3.1.2. Fidelity

(A) Low fidelity: In the initial phases of the design, these models are extensively employed to establish the preliminary sizing and formations for FOWTs. They typically rely on steady-state, quasi-static, or static analyses. Examples of low-fidelity models used in this context are analyses focused on hydrostatic stability and equilibrium, hydrodynamic assessments in the frequency domain, empirical methodologies, and simplified state-space models. These models are crucial for setting initial parameters and configurations in the design process.

(B) Medium fidelity: In the phases of design validation and optimization, these models are employed to primarily capture the essential behaviors of FOWTs. The models are designed to be less detailed, prioritizing speed over precision in simulations during these critical design stages. Techniques such as model testing, forced oscillation, and comprehensive aero-hydro-servo-elastic simulations are typical examples of partially coupled methods included in this approach. These methods strive to achieve an optimal balance between rapid simulation capabilities and the necessary accuracy for effective design evaluation.

(C) High fidelity: These are the models employed during the ultimate phase of design verification. The core governing equations are implemented with minimal simplifications. Due to their complexity and the time required, these methods are primarily utilized to refine the design. High-fidelity approaches include coupled FEM and CFD simulations, as well as real-time hybrid simulations (RTHSs). These advanced methods offer detailed insights essential for precise design adjustments.

Furthermore, the methods mentioned in Figure 9 are categorized according to their fidelity levels in Table 4.

Table 4. FOWT numerical methods and their fidelity.

References	Methods	Fidelity	Category
[77]	Boundary Element Momentum Theory (BEMT)	Mid	Aerodynamic
[78]	Potential Flow (PF)	Mid	Aero-/hydrodynamic
[79]	Free Vortex Wake Method (FVW)	Mid	Aerodynamic
[80]	Generalized Dynamic Wake Method (GDW)	Mid	Aerodynamic
[81]	Finite Element Method (FEM)	High	Structural
[82]	Quasi-Static Method (QS)	Low	Structural
[83]	Dynamic Method (Dyn)	Mid	Structural
[84]	Morison Equation (ME)	Mid	Hydrodynamic
[85]	Boundary Element Method (BEM)	Mid	Hydrodynamic
[86]	Computational Fluid Dynamics (CFD)	High	Aero-/hydrodynamic

3.1.3. Software

Analysis programs designed for FOWTs employ specialized components to tackle different aspects such as mooring dynamics, structural dynamics, hydrodynamics, and aerodynamics. The structural dynamics components simulate the flexible segments of the FOWTs, which can be modeled with rigid components, modal foundations, multibody systems integrated with dampers and springs, or the FEM. Aerodynamic forces are evaluated using methods like BEMT, GDW, or dynamic stall models. For hydrodynamic analysis, a hybrid methodology is often utilized, combining PF theory with ME. Mooring dynamics are represented using QS models, lumped mass strategies, or the FEM. Tables 5 and 6 provide a detailed comparison of the abilities of numerous engineering analysis programs for FOWTs, and list several of the most widely recognized high-fidelity programs in the field.

Table 5. Capabilities for modeling in various engineering software.

References	Code	Structure	Aerodynamics	Hydrodynamics
[74]	HAWC2	Dyn + FEM	GDW + BEMT	ME + PF
[75]	OpenFAST	FEM/Modal + QS/Dyn + RB	FVW/GDW + BEMT	ME + PF
[76]	Bladed	Modal	GDW + BEMT	With SIMA
[87]	Orcaflex	FEM + RB + Dyn	With OpenFAST	ME + PF
[88]	Flexcom	FEM + RB + Dyn	With OpenFAST	ME + PF
[89]	SIMPACK	FEM	AeroModule/AeroDyn	With HydroDyn
[90]	SIMA	Dyn + FEM	BEMT	ME + PF

Table 6. High-fidelity software.

References	Code	Numerical Method
[91]	OpenFOAM	CFD
[92]	Ansys	FEM + CFD
[93]	Abaqus	FEM + CFD
[94]	Star CCM+	CFD
[95]	CFDShip-Iowa	CFD
[96]	Code Saturne	CFD
[97]	REEF3D	CFD

3.2. Hydrodynamics

Numerical modeling techniques for fluid dynamics challenges have primarily evolved from maritime and offshore oil and gas sectors but are also relevant to FOWT platforms [98]. PF methods, ME, or a hybrid of both, are employed to compute wave excitations of the first and second order. These mid-fidelity methods generally provide a good balance between accuracy and computational efficiency but may encounter difficulties with intricate shapes where the flow interference among components is not adequately addressed. The PF technique [99] is utilized to determine the diffraction and radiation forces. The drawbacks of PF include disregarding viscous forces and assuming minor vibration amplitudes compared to the floating structure's cross-sectional area. Numerical applications based on PF theory utilize the BEM, which segments the floating structure into sections, calculating fluid dynamics forces by integrating dynamic pressure across these submerged sections. For frequency-domain PF solvers, the submerged form is established at hydrostatic equilibrium in still water. In contrast, time-domain PF solvers often require pre-processed hydrodynamic coefficients from frequency-domain PF solvers to establish the submerged structure sections [26]. ME is typically employed for frameworks with slender cylindrical components. It computes both inertial and viscous forces, making it suitable for structures exposed to waves and currents, unlike PF, which only accounts for inertial forces. ME, initially introduced by Morison et al. [84] for stable, elongated cylindrical offshore structures, is also applicable to FOWTs. However, ME does not consider changes in the wave pattern caused by the floating entity. A hybrid strategy using PF methods and ME is implemented when a single method alone cannot encompass all hydrodynamic effects. This combined strategy is a computationally efficient alternative to complete the CFD modeling [100], particularly valuable for FOWT platforms with substantial columns and thin supports, or when viscous drag impacts are significant in harsh marine environments.

High-fidelity CFD models [101] solve complex flow problems using the Navier–Stokes equation (NSE). CFD is generally employed for particular nonlinear issues, such as impact loads from massive waves and detailed flow dynamics like vortex shedding near heave plates. Additionally, CFD models can fine-tune parameters for lower-fidelity models numerically, serving as an alternative to physical decay tests [102]. Comparing CFD models directly with PF + ME models is complex [103]. The accuracy of each model depends on various factors, including the load cases, whether steady-state or transient equations are utilized for CFD, the tuning of hydrodynamic coefficients, mesh characteristics, user expertise, and ensuring a converged solution. Achieving accurate results with PF + ME

solutions requires several components, such as calculating second-order PF solutions, wave stretching (considering wave forces beyond the free surface), and incorporating proper viscous damping, especially when second-order PF forces are considered.

3.3. Aerodynamics

One of the most complex aspects of airflow dynamics for FOWTs involves changes in relative wind speed due to the platform's motion [104,105]. This phenomenon, known as dynamic inflow or unsteady dynamics, can lead to an increase in rotor thrust loading, also known as negative damping. Mid-fidelity, quasi-steady BEMT models [106] struggle with accurately representing the dynamic inflow [107]. BEMT merges the momentum and blade element theories, segmenting turbine blades into smaller divisions. The airflow characteristics for each division are determined individually, and the overall rotor characteristics are obtained by integrating these values. Quasi-steady BEMT models presume the immediate balance of the turbine wake. Research, including studies by Henriksen et al. [108] and Ferreira et al. [109], indicates that integrating a straightforward dynamic inflow model enables BEMT models to effectively represent dynamic inflow effects while keeping computational proficiency.

Advanced models utilizing PF and CFD techniques [110,111] can address dynamic inflow, although this comes with a trade-off in computational speed. Recently, simulation tools have started to include the FVW technique for airflow modeling [112,113]. With the growth in rotor dimensions, it is increasingly crucial to accurately model airflow disturbances caused by significant blade bending. The FVW technique offers a compromise in terms of precision and computational speed between the CFD and BEMT methods. This method provides in-depth wake modeling, which influences airflow dynamics on the rotor, through Lagrangian vorticity discretization. The FVW technique has been incorporated into OpenFAST and other industry software [114]. Additionally, the progression of the turbine wake and its influence must be evaluated for their impact on FOWT dynamics, downwind turbines, and wind farm configuration [115,116]. As mentioned earlier, choosing the right numerical method during the design stages requires balancing the available resources and time against the desired levels of precision and reliability in the model. Other factors include the specific load scenarios to be investigated, the particular FOWT configuration, and the current stage of the design process, whether in initial assessments or detailed analyses.

3.4. Structural Dynamics

The evolution from low to high fidelity in the structural modeling of FOWTs depends on the scope, variety, intricacy, and precision of the responses they effectively address. Low-fidelity models, in their simplest configuration, capture the overall rigid-body movements or the actions of individual rigid components, making them suitable for comprehensive stability evaluations but not for intricate deformation analysis [117]. These models are particularly advantageous for early-stage, rapid conceptual designs or evaluations. Sometimes, certain segments of the system may be modeled stiffly while others are treated as flexible. Mid-fidelity models are commonly characterized by components such as beams, cables, and connectors, possessing both linear and nonlinear characteristics [118]. These models have been utilized to analyze aerodynamic consistency and predict dynamic outcomes concerning deformation and material properties [119–121]. They are formulated using differential equations and can be validated through scaled model tests, as a result of their non-dimensional forms. Numerical implementation can incorporate factors such as damage due to chemical or physical influences (e.g., corrosion) and biological accretions [122,123]. These mid-fidelity models are also essential for evaluating safety concerning fatigue and ultimate limit states (ULSs) via standardized evaluations [124]. Static analysis is used in the initial design phase to assess loads, while time-domain modeling is necessary later to examine fatigue and significant loads under varying operational, severe, and fault/start-up scenarios.

A prevalent technique in structural dynamics is the modal method, wherein certain flexible DOF are characterized by their modes and mode shapes. This technique is employed, for instance, to simulate blades and towers using FAST. At the most comprehensive fidelity

level, FEM is applied to depict one or all aspects of the structure, encompassing the platform, tower, blades, and mooring lines [125,126]. Different elements of the system are often modeled with varying levels of fidelity based on the analysis goals and the comparative flexibility of the elements. FEM models involve numerous DOF, and dimensional reduction is frequently necessary in order to enhance computational efficiency [127]. For linear assessments or approximations, a modal superposition method often yields a reliable response prediction utilizing state-space models [128]. However, the effectiveness of these models depends on precisely selected system parameters and suppositions regarding the physics and loading excitation. Deviations from these suppositions can result in notable errors, as the response data are expressed through a limited set of generalized modal coordinates.

Reduced DOF can also be obtained by calculating the rigid body kinematics of structural components and integrating them with pre-calculated elastic properties to estimate deformations [38]. The BEM is another method frequently utilized for understanding fluid–structure interactions, typically involving low-order meshing appropriate for rigid structures [129–131]. Recently, the finite volume method (FVM) in a Simo–Reissner format has been applied to significantly deformable structures [132,133]. The dynamic nonlinear properties of mooring lines and power cables, including their long-term effects, interconnections, buoyancy elements, and ballasting impacts, are active research areas [134]. Traditional quasi-static models, computed based on the correspondence of relevant parameters at each time step, are employed for mooring dynamics due to their computational simplicity. However, these models tend to underpredict restoring forces, especially in severe sea conditions, and are less effective for platforms with catenary moorings and natural frequencies close to peak wave frequencies [135,136]. Dynamic analyses, despite higher computational demands, are preferred as they more accurately reflect experimental results. Efforts to enhance computational performance in these methods, including frequency-domain techniques, are ongoing [137,138]. Structural modeling has evolved to include complexity and detail, capturing a wide range of phenomena, responses, and stochastic elements across different spatial and temporal scales through various discretization techniques. Over time, the focus on computational simplicity has diminished with the growth of computing capabilities and the increased availability of large-scale computing resources for such analyses.

4. CFD Modelling for FOWT Analysis

4.1. CFD-Based Aerodynamics and Hydrodynamics

The dynamics of fluid flow around FOWTs can be most precisely described by resolving the NSE using CFD techniques [139]. These equations can be adapted to both incompressible and compressible flow scenarios, depending on the physical characteristics and the flow conditions of the study.

Compressible Flow

For scenarios where the fluid density varies significantly with pressure or temperature, such as high-speed gas flows, the NSE are modeled for compressible flow:

The continuity equation is as follows:

$$\frac{\partial \rho}{\partial t} + \nabla \cdot (\rho u) = 0 \tag{1}$$

where ρ is the fluid density and u is the velocity vector of the fluid.

The momentum equations are as follows:

$$\frac{\partial (\rho u)}{\partial t} + \nabla \cdot (\rho u \otimes u) = -\nabla p + \nabla \tau + \rho f \tag{2}$$

where p is the pressure, τ is the stress tensor, and f represents body forces

Incompressible Flow

In scenarios where the fluid density does not significantly change, such as in many hydrodynamic and aerodynamic applications related to FOWTs, the fluid is modeled as incompressible. The incompressible NSE include the following:

The continuity equation is as follows:

$$\nabla \cdot u = 0 \tag{3}$$

The momentum equations are as follows:

$$\frac{\partial u}{\partial t} + (u \cdot \nabla)u = -\frac{1}{\rho}\nabla p + \nu \nabla^2 u + f \tag{4}$$

where ν represents the kinematic viscosity ($\nu = \frac{\mu}{\rho}$), and μ is the dynamic viscosity.

In the modeling of FOWTs, the assumption of incompressible flow is extensively utilized for both hydrodynamic and aerodynamic simulations. For hydrodynamics, this assumption is justified by the properties of water and the low flow velocities typically encountered around the turbine structures. These lower velocities mean that the water's density remains relatively constant, making it feasible to treat the water as an incompressible fluid [78]. For aerodynamics, considerations of compressible flow become necessary only if Mach numbers approach or exceed 0.3 [140]. However, the operational speeds of wind turbine blades typically result in Mach numbers below this threshold. Therefore, incompressible flow models are effective and accurate for both air and water interactions with FOWTs, facilitating precise simulations of load predictions, motion responses, and overall turbine dynamics [24,34,103,111,139]. This approach simplifies the analysis process while ensuring an efficient and accurate assessment of FOWT performance.

The accurate aerodynamic analysis of FOWTs relies heavily on precise turbulence modeling around the turbines [141]. For turbulent flow conditions, CFD uses three primary methods to solve the NSE (unsteady Reynolds-averaged Navier–Stokes (RANS) equations, large eddy simulation (LES), and direct numerical simulation (DNS)). DNS, when accurately implemented, resolves turbulence up to the Kolmogorov scale with a very fine grid [142], which is impractical due to its extremely high computational cost. Therefore, RANS and LES are generally employed to either fully or partially simulate the effects of turbulence in the flow [143].

LES captures the dominant energetic large eddies and parameterizes the effects of smaller eddies, which have more universal properties, using a subgrid-scale model (SGS) [144]. LES employs a spatial filter to separate the scales into large eddies and small eddies [145]. Using this filter modifies the NSE in the following way:

$$\frac{\partial \widetilde{u}_i}{\partial x_i} = 0 \tag{5}$$

$$\frac{\partial \widetilde{u}_i}{\partial t} + \widetilde{u}_j \frac{\partial \widetilde{u}_i}{\partial x_j} = -\frac{1}{\rho}\frac{\partial \widetilde{p}}{\partial x_i} + \nu \frac{\partial^2 \widetilde{u}_i}{\partial x_j \partial x_j} - \frac{\partial \tau_{ij}}{\partial x_j} + \widetilde{f}_i \tag{6}$$

where the variables $\widetilde{p}$ and $\widetilde{u}_i$ represent the pressure and filtered components of velocity. The term τ_{ij} represents the SGS stress tensor that emerges in the NSE as a result of spatial filtering. This tensor accounts for the effects of the unresolved smaller eddies. The Smagorinsky model is the most prevalent method for computing τ_{ij} [146]:

$$\tau_{ij}^{\text{model}} \approx -2\nu_t \widetilde{S_{ij}} + \frac{1}{3}\tau_{kk}\delta_{ij} \tag{7}$$

where ν_t represents the eddy viscosity, defined based on the resolved velocity field; $\widetilde{S_{ij}}$ is the filtered strain rate tensor, defined as $\widetilde{S_{ij}} = \frac{1}{2}\left(\frac{\partial \widetilde{u}_i}{\partial x_j} + \frac{\partial \widetilde{u}_j}{\partial x_i}\right)$; and δ_{ij} is the Kronecker delta. Nevertheless, this model fails to address secondary flows and anisotropy in turbulence because it relies on the Boussinesq hypothesis [147,148]. To overcome such shortcomings, various additional SGS turbulence models have been suggested, including dynamic

Smagorinsky models, anisotropic minimum dissipation models, scale-dependent dynamic models, and mixed SGS models [149,150].

Given the rigorous requirements of LES for grid refinement in all three spatial dimensions near solid surfaces to effectively model the turbulent boundary layer, its application to turbine blades is typically deemed impractical. Consequently, LES is more commonly utilized for modeling the wakes of turbines, where the turbine rotor is represented through various actuator techniques such as the actuator surface (AS), actuator line (AL), and actuator disk (AD) depicted in Figure 10 [151–153]. The adoption of actuator techniques significantly reduces computational expenses by foregoing the detailed resolution of the boundary layer adjacent to the blades. Additionally, to lessen the computational load of LES, hybrid RANS-LES approaches are adopted, where the RANS equations model the boundary layer close to the surface, and LES is applied to the unsteady separated regions that are distant from the surface [154–157].
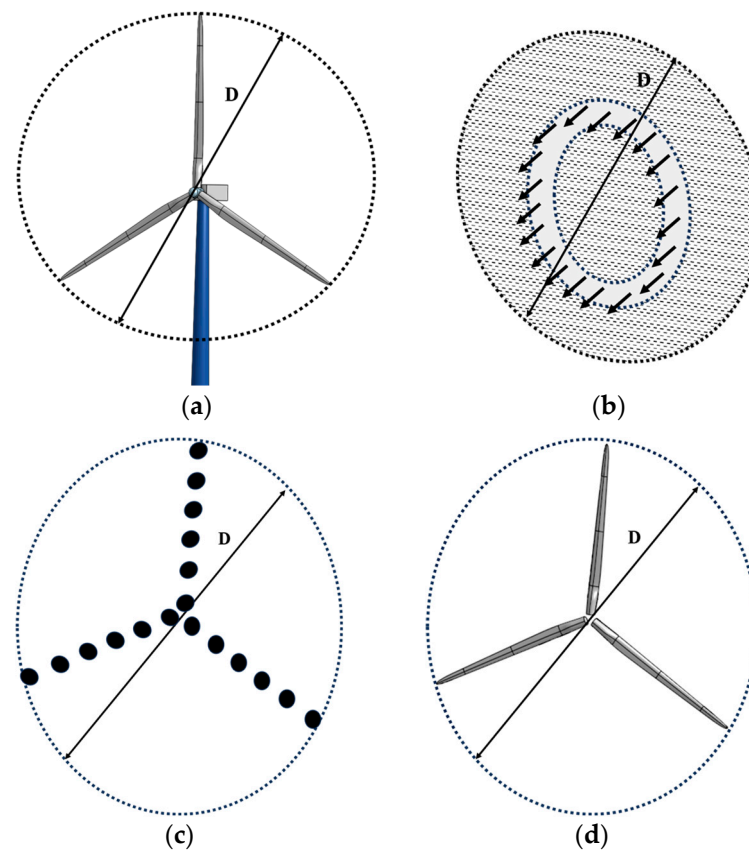

(a)

(b)

(c)

(d)

Figure 10. Wind turbine actuator representations for aerodynamics: (**a**) wind turbine, (**b**) AD, (**c**) AL, and (**d**) AS. Note: In the figure, the symbol D represent diameter.

Simulations utilizing RANS equations are among the most common methods for assessing turbine aerodynamics with CFD techniques [158,159]. Likewise, hydrodynamic forces exerted on FOWTs are typically determined using RANS equations combined with a turbulence model, computed numerically via the FVM [160–162]. The equations known as RANS, derived from the collective averaging of the NSE equations, are presented thus [163]:

$$\frac{\partial \overline{u}_i}{\partial x_i} = 0 \tag{8}$$

$$\frac{\partial \overline{u}_i}{\partial t} + \overline{u}_j \frac{\partial \overline{u}_i}{\partial x_j} = -\frac{1}{\rho} \frac{\partial \overline{p}}{\partial x_i} + \nu \frac{\partial^2 \overline{u}_i}{\partial x_j \partial x_j} - \frac{\partial \overline{u'_i u'_j}}{\partial x_j} + \overline{f}_i \tag{9}$$

where $\overline{p}$ and $\overline{u}_i$ represent the ensemble pressure and components of mean velocity, varied with spatial coordinates (x_i) and time (t). The symbols ν and ρ correspond to kinematic viscosity and fluid density, respectively. The Reynolds stress tensor $\overline{u'_i u'_j}$ captures the effects of turbulence. It is frequently modeled with the eddy viscosity (EV) technique which relies on the Boussinesq hypothesis [164]:

$$\overline{u'_i u'_j} = -\nu_t \left(\frac{\partial \overline{u}_i}{\partial x_j} + \frac{\partial \overline{u}_j}{\partial x_i} \right) + \frac{2}{3} k \delta_{ij} \tag{10}$$

where k denotes turbulent kinetic energy and ν_t refers to the EV. The EV could be resolved without resolving extra transport equations, as in Prandtl's mixing-length model [165]. More advanced turbulence models (one-equation and two-equation) have been created to compute EV more precisely [166–168]. The models (e.g., two-equation) $k - \omega$ shear stress transport (SST), and $k - \varepsilon$ are the most widely used for hydrodynamic assessments of FOWTs [169,170], solving two transport equations to model turbulence. For aerodynamic assessments of FOWTs, the models (two-equation), notably, $k - \omega$ SST and $k - \omega$, are also popular [171–175]. However, these models, relying on the Boussinesq hypothesis, cannot capture turbulence anisotropy [176,177]. Therefore, more advanced models such as realizable models, Reynolds stress turbulence (RST) models, and nonlinear EV models are advised for precise aerodynamic load predictions [178–180]. RSMs provide the most accurate results by solving separate transport equations for each Reynolds stress component, although they demand more computational resources [181]. Nonlinear cubic and quadratic EV models offer a more cost-effective alternative, effectively capturing turbulence anisotropy. To further decrease computational demands, actuator methods are commonly utilized to represent turbine rotors in the RANS framework [182–185].

In addition to deterministic methods, it is critical to incorporate stochastic methodologies to account for the random processes inherent in the marine environment. Stochastic differential equations (SDEs) can be employed to simulate the variability in environmental loads such as wind and waves, integrating these random fluctuations directly into the NSE [186,187]. Furthermore, Monte Carlo simulations can assess the probabilistic responses of turbine structures to these loads, enhancing the reliability analysis of FOWTs [188,189]. For non-stationary random processes, methods such as empirical mode decomposition provide insights into the time-varying nature of environmental inputs, offering a dynamic perspective on load modeling [190]. Additionally, advanced turbulence models that consider the stochastic nature of turbulence can be integrated into the CFD framework, thereby improving the accuracy of flow simulations around FOWTs [191,192]. These enhancements are crucial for developing robust designs that can withstand the unpredictable ocean environment, ensuring both the efficiency and safety of wind energy systems.

To represent the free surface in CFD, two primary techniques are utilized: interface-capturing and interface-tracking. The interface-tracking technique, as indicated by its name, follows the free surface using a Lagrangian grid that conforms to the interface. However, when the interface undergoes significant motions, tracking becomes challenging and requires remeshing techniques. This approach not only increases computational demands but also can lead to errors in the numerical solutions. Conversely, the interface-capturing technique, also known as the Eulerian grid method, locates the free surface by calculating the volume within a computational domain that encompasses the free surface. Unlike the interface-tracking technique, this method does not require the grid to follow changes in the free surface over time.

For modeling the free surface in FOWTs, the level set and volume of fluid (VOF) methods are most commonly employed, both of which are categorized as interface-capturing techniques [193–195]. Capturing the free surface profile with these methods requires an increased cell density near the interface. This is typically achieved by using a specific number of cells aligned perpendicular and parallel to the free surface for spatial discretization [196]. Enhanced cell concentration at the free surface can also be influenced by kinetic

wave energy [197]. To prevent wave reflection at the edges of the numerical domain, two methods are used. One method dampens the waves by making the grid course toward the edges [196]. Another strategy utilizes a damping (relaxation) function within a relaxation zone near the edges to steer the wave field towards an uninterrupted free surface [198].

4.2. FOWT CFD Analysis

4.2.1. Uncoupled Analysis

In the field of fluid–structure interactions and wind turbine analysis, numerous studies have concentrated on uncoupled simulations to describe and understand different hydrodynamic and aerodynamic behaviors. These investigations commonly utilize CFD tools to simulate the performance of FOWTs. Uncoupled analysis, in this context, refers to the separate examination of hydrodynamic and aerodynamic forces acting on the structure, without accounting for their mutual interactions in a single coupled framework. This approach allows researchers to focus on specific aspects of the FOWT's behavior under various conditions, making it a valuable tool for preliminary analysis and design optimization.

While uncoupled analysis offers the advantage of simplicity and reduced computational cost, it has limitations. It may not accurately capture the combined effects of wind and wave forces, potentially leading to oversimplified results. Nevertheless, it provides detailed insights into specific phenomena, laying the groundwork for more advanced coupled analyses. Table 7 highlights the existing studies based on uncoupled analysis, showcasing the methodologies and findings that have significantly contributed to the understanding of FOWT dynamics.

Table 7. Uncoupled models summary.

References	Tools	Key Findings
[169]	Open-source CFD code ReFRESCO	Conducted analysis of surge decay for the platform (OC5 DeepCwind).
[163]	OpenFOAM	Verified the results of regular wave and free decay tests for the platform (OC5 DeepCwind) by comparing them with established literature.
[160]	STAR-CCM+	Executed regular wave and free decay testing on the model (OC4 DeepCwind).
[199]	STAR-CCM+	Increased fatigue load at lower wind speeds; effect diminishes at higher speeds.
[200]	ANSYS-FLUENT	Evaluated aerodynamic power and thrust for wind speeds 8 m/s to 25 m/s.
[201]	ANSYS-FLUENT	Significant aerodynamic load on the tower due to blade rotation.
[171]	STAR-CCM+	Comparable power and thrust coefficients at full scale and model scale (1/50).

4.2.2. Partially Coupled Analysis

CFD simulations were performed on the system with simplified dynamics by accounting for specified movements in certain DOF. The majority of the CFD studies listed in Table 8 employed the overset meshing technique, which consists of a background grid combined with a refined overlapping mesh approach. The phenomena exhibited by the FOWTs during forced oscillations are outlined in Table 8. The surge and pitch DOF of the platform significantly affect the aerodynamic behavior of the FOWTs [117,202]. These DOF, together with yaw, lead to uneven and angled wind forces on the rotor [91]. Wen et al. [203] used the free vortex approach to examine how surge dynamics influence the power and thrust properties of the wind turbine (National Renewable Energy Laboratory (NREL) 5MW). The study applied surge dynamics with varying amplitudes (0 m to 2.5 m) and frequencies (0 Hz to 0.2 Hz) on the FOWTs. The results showed that power output diminishes at lower tip–speed ratios (TSRs) and rises at higher TSRs. Jeon et al. [204] investigated the aerodynamic conditions of the wind turbine (NREL 5MW) model exposed to platform pitching motions using the vortex lattice method (VLM). They noted tip vortex shedding when the platform pitches in the upwind direction. The VLM considered the wake generated by the turbine and its corresponding non-induced effects. Further examples in the literature is summarized in Table 8.

Table 8. Partially coupled model's summary.

References	Tools	Key Findings
[110]	OpenFOAM	Discrepancies observed between FAST/BEM outcomes and CFD method predictions for large-scale platform motions and elevated frequencies.
[205]	ANSYS-FLUENT	Alterations in mean thrust force attributable to surge dynamics; intense interactions between rotor wake and frequencies and higher surge amplitudes.
[206]	OpenFOAM	Dependence of blade twist on the occurrence of propeller states along the blade radius; adjustments in wind angle attack leading to negative lift coefficients.
[111]	OpenFOAM	A 5% reduction in aerodynamic thrust and power due to blade elasticity; fluctuations in aerodynamic power and thrust resulting from variations in angle and wind speed.
[207]	STAR-CCM+	Instability of blade tip vortices and significant interactions with the tower triggered by surge movements; modifications in the stall angles of airfoil sections due to surge dynamics and wake interactions varying by amplitude and frequency.
[208]	STAR-CCM+	Sensitivity of changes in aerodynamic power and thrust coefficients due to pitching movements is 12 to 16 times greater than those caused by yawing.
[209]	STAR-CCM+	Fluctuations in wake strength due to platform's oscillatory movements; augmentation of blade–wake interactions with increases in displacement amplitude and angular frequency.
[210]	STAR-CCM+ and ANSYS-FLUENT	Pitching movements lead to variations in additional velocities on rotor blades, altering non-axial wind angles; enhanced aerodynamic power and thrust as pitching amplitude escalates.
[16]	ANSYS-FLUENT	High-frequency oscillations in surge and pitch DOF result in greater power and thrust fluctuations due to induced velocity changes; elevated thrust observed in platform pitching movements compared to surging; intensified vortex activity under combined surge–pitch dynamics.

4.2.3. Fully Coupled Analysis

(A) Aero-Hydro-mooring: In comparison to predefined platform movements, fully integrated aero-hydrodynamic behaviors of FOWTs influenced by prevailing wind and waves are more representative. Ren et al. [211] developed an integrated dynamic model (5MW TLP) utilizing Fluent software, confirming their findings with experimental evidence. They concluded that hydrodynamic forces primarily govern the dynamic surge motion, while aerodynamic loads mainly influence the average surge value. Tran and Kim [24] devised a computational model for the integrated aero-hydrodynamics of a semi-submersible FOWT using STAR CCM+ with the overset mesh technique. Figure 11 illustrates the domain and mesh distribution of the FOWTs. They identified a notable discrepancy of 19.6% in surge response between FAST code and CFD, while pitch and heave responses were more aligned across both methods. They observed that the unsteady aerodynamic performance predicted by FAST needs more examination due to significant differences when utilizing various aerodynamic approaches. Specifically, the variations in thrust coefficient for BEM and GDW were 24.0% and 33.3%, respectively, relative to CFD results. In another study, Tran and Kim [212] employed a similar approach in order to analyze the interactions of aero-hydro-mooring–wake dynamics in an FOWT. They visualized blade tip vortices and vortices detaching from the hub, tower, and platform, as displayed in Figure 12. Zhang and Kim [213] performed an integrated CFD analysis for a semi-submersible FOWT, disclosing that the rotor thrust was 7.8% higher than that of an onshore wind turbine, while the rotor power was reduced by 10%, likely due to the reduced windward area and relative wind speed from the inclined platform. Quallen and Xing [214] address the 6-DOF motions of the FOWTs and implemented a variable speed generator-torque controller to manage power generation. Increased mooring forces were shown to aid in keeping the FOWTs within an optimal variable speed control range. Liu et al. [215] examined the dynamic responses of a semi-submersible FOWT with pitch, heave, and surge DOF using the sliding mesh technique to accommodate the relative movement between the rotating turbine and

the platform. They noted that mooring tension forces were significantly amplified by the substantial platform surge response. Zhou et al. [216] investigated the dynamic responses of an FOWT under three types of incident waves: the irregular wave, focused wave, and reconstructed focused wave. They observed that hydrodynamic characteristics stimulated by reconstructed focused and irregular waves were comparable, but both displayed significant deviations from focused waves. Additionally, tower bending moments and mooring tension forces exhibited dynamic responses at multiple frequencies, correlating with the first-, second-, and higher-order natural frequencies of the structure, highlighting the system's nonlinear characteristics. Feng et al. [217] created an integrated model based on CFD, using the dynamic fluid body interaction (DFBI) method. They conducted several integrated dynamic simulations under power production, shutdown, and startup conditions. The results from the power production scenario showed that blade pitch motion reduces aerodynamic loads and raises the response amplitude of the platform, introducing negative damping into the FOWT system. Simulations for shutdown and startup scenarios revealed that extreme motion responses are intensified, and mooring line tension fluctuates once in a high-tension state.
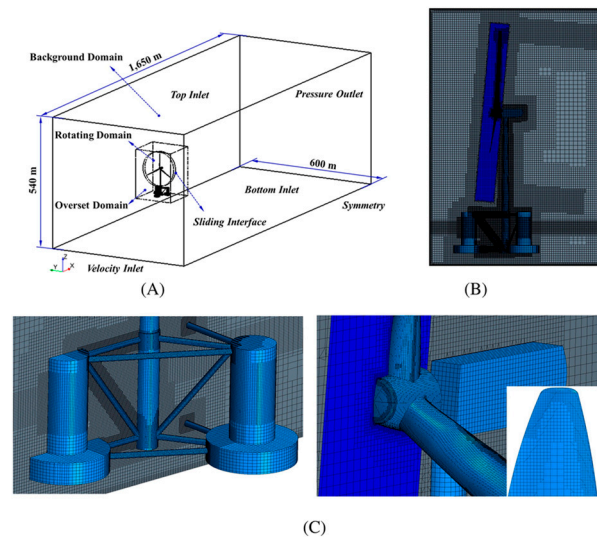

Figure 11. FOWT computational mesh. (**A**) Computational domain, (**B**) entire turbine model with overset region, and (**C**) close view of turbine parts and platform surface mesh. Adapted with permission from [24], John Wiley and Sons, 2017.
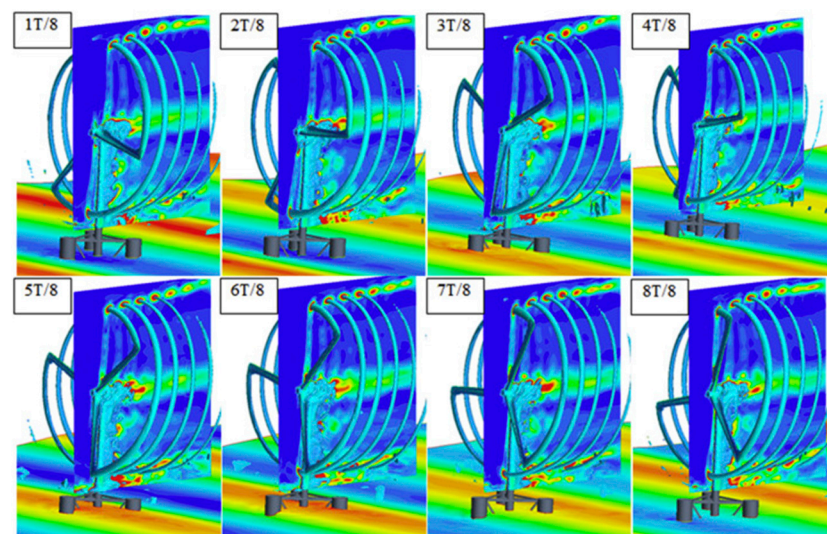

Figure 12. FOWT vorticity contours. Adapted with permission from [212], Elsevier, 2016.

Blade-resolved modeling for integrated aero-hydrodynamic simulations of FOWTs requires substantial computing power. To tackle this, Cheng et al. [218] introduced a unique solver (FOWT-UALM-SJTU) based on CFD, which merges the unsteady actuator line method (UALM) with their proprietary CFD solver (naoe-FOAM-SJTU), to effectively simulate platform hydrodynamics. Their research focused on the integrated behavior of the wind turbine (NREL 5 MW) on a semi-submersible platform. In a related study, Huang et al. [219] utilized the UALM in their solver (FOWT-UALM-SJTU), to simulate the wind turbine's dynamics. Their investigation comprehensively assessed the interactions between the wind turbine and the spar-buoy platform under simultaneous wind and wave influences, considering various platform DOF and turbine operational states. Their findings indicated that the aerodynamic forces significantly intensified the platform's pitch and surge movements, whereas the heave motion was reduced by the rotor's vertical thrust component.

(B) Aero-Hydro-Elastic-mooring: To investigate rotor–wake dynamics in FOWTs, Rodriguez and Jaworski [220] integrated the FVM within an aeroelastic computational framework featuring robust bi-directional interaction between the fluid and structural domains. Due to a shortage of aeroelastic experimental benchmarks for FOWTs, validation processes for aerodynamic efficiency and structural integrity were conducted using separate sets of experimental data. This validated model was subsequently used to analyze rotor–wake dynamics and aeroelastic properties of FOWTs across a range of operational scenarios [221]. This integrated model using FVM provides reliable predictions for wind turbine aerodynamics in complex environments; it faces challenges in modeling flow detachment on blade surfaces, lacking fluid viscosity effects. Therefore, further validation is essential, especially for intricate aeroelastic simulations of FOWTs. Advanced CFD tools are crucial for exploring the comprehensive aero-hydro-elastic performance of these turbines. Liu et al. [111] combined an advanced CFD solver with the structural analysis tool MBDyn to evaluate aeroelastic responses under controlled surge motion scenarios. MBDyn computes blade deformations from the fluid dynamics predictions made by the solver pimpleDyMFoam, and these deformations are reintroduced into the fluid dynamics model through an updated mesh. Their studies highlighted the detrimental effects of blade deformations on aerodynamic efficiency and examined the impact of surge motion on the behavior of flexible turbine blades, noting that surge motion intensifies variations in rotor thrust and power output. They also developed an integrated aero-hydro-elastic simulation tool for FOWTs in combined wave and wind conditions [222], which was validated using data from semi-submersible FOWTs to examine blade deformations, aerodynamic effects, platform movements, and mooring line tensions.

Owing to the substantial computational demands of blade-resolved CFD analyses, Yu et al. [223] examined the aeroelastic behaviors of the wind turbine (NREL 5 MW) under both isolated and complex interaction scenarios using the actuator line model (ALM) integrated with a beam solver. Their findings highlighted that blade flexibility amplifies the impact of tower shadows and introduces stability challenges. In a subsequent project, Yu et al. [224] formulated a composite numerical model employing the potential–viscous flow model qaleFOAM, aimed at stimulating the interconnected dynamics of FOWTs. This model emphasized the complex interplay between the aero-elastic-hydro-mooring–wake dynamics. In their simulations, turbine components such as the blades, hub, and tower were depicted through respective actuator lines, as shown in Figure 13a, with the domain's computational mesh illustrated in Figure 13b. Their analyses demonstrated that the predictions of aerodynamic efficiency, blade tip displacement, platform movement, and mooring cable stresses aligned well with outcomes from alternative approaches. Additionally, they noted that the model effectively captured the interdependent dynamics among blade deformations, platform movements, and wake flows, as evidenced in Figure 14.
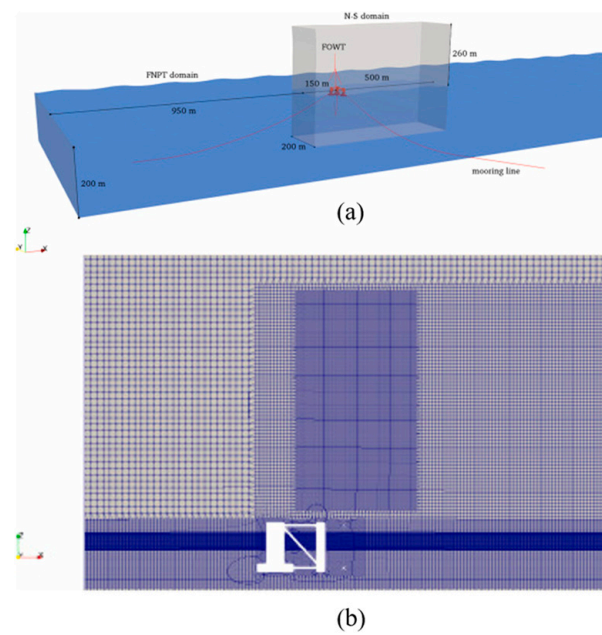
Figure 13. (**a**) Sketch of FOWT domain and (**b**) computational grid for the domain. Adapted with permission from [224], Elsevier, 2023.
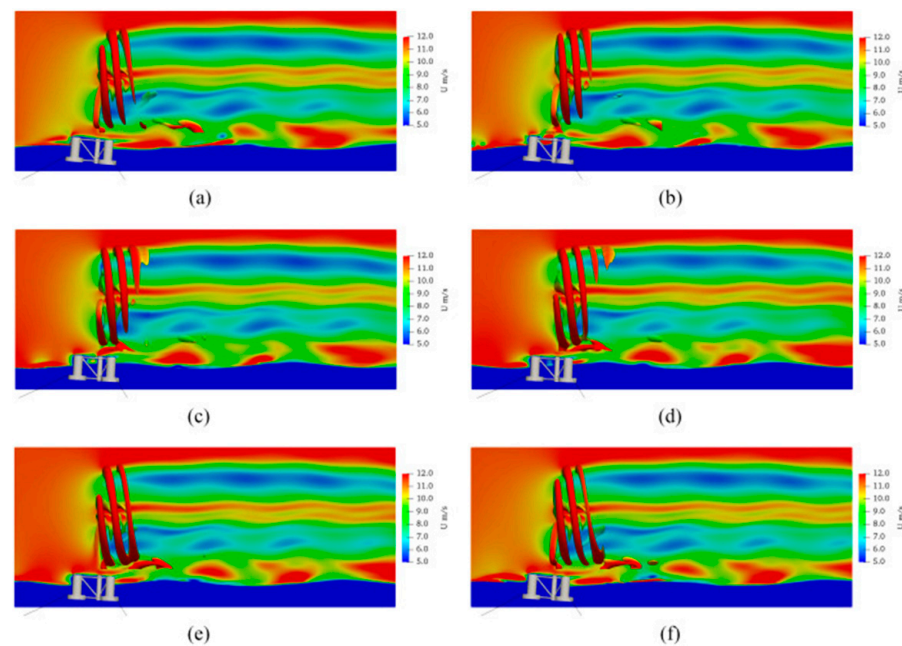

Figure 14. Flow field and vortex close to wind turbine: (**a**) T/6; (**b**) T/3; (**c**) T/2; (**d**) 2T/3; (**e**) 5T/6; and (**f**) T. Adapted with permission from [224], Elsevier, 2023.

(C) Other Coupled Models: In FOWT dynamic analysis, the coupling of numerous numerical models plays a critical role in accurately predicting system responses under different environmental conditions. Beyond the initial models discussed, several other sophisticated coupling schemes have been developed to further enhance our understanding and capability in this area. The specifics of these models, including their applications and the distinct methodologies employed, are detailed in Table 9. This table provides an essential overview of these coupled models, highlighting their unique contributions to the field of FOWT research.

Table 9. Summary of other coupled numerical models.

References	Coupling Scheme	Model Description
[225]	CFD-BEM-MBD	Coupled CFD model with aero-servo-elastic OpenFAST code for simulating OC4 DeepCwind FOWTs dynamic responses.
[226]	CFD-PF	Introduced a coupled fluid–structure interaction approach utilizing LES to examine FOWT behaviors in wave environments. The analysis domain is segmented into a near-field area employing a two-phase LES solver and a far-field zone utilizing an aerodynamic LES model, which integrates non-viscous dynamics with PF.
[227]	CFD-PF-MBD	Explored the wake dynamics of the FOWT (OC4 semi-submersible) compared to its fixed-base version under atmospheric boundary layer (ABL) conditions through an AL method employing the SOWFA LES solver.
[228]	Linear diffraction theory and FEA	Investigated the hydro-elastic properties of an innovative triangular floating platform designed to support three wind turbines at its corners.
[229]	Coupled linear PF-FEA	Assessed the potential collision between ships and FOWTs. The aerodynamic thrust force is modeled as a point load at the turbine hub, derived from the thrust curve for the wind turbine (NREL 5 MW).

5. Challenges and Recommendations

5.1. Modeling Turbulence and Atmospheric Interactions

One critical issue in CFD simulations of FOWTs is the selection of a suitable turbulence model. Typically, these simulations are conducted using RANS equations, with the $k - \omega$ SST model being the most popular due to its reliability and efficiency. This model, along with the Spalart–Allmaras model, depends on the Boussinesq approximation, which, unfortunately, overlooks turbulence anisotropy, and this can be a significant limitation as it may not fully capture the complex flow characteristics around the turbines. To address this, it is advisable to consider nonlinear EV models, which represent a promising alternative. These models provide improved precision in capturing the turbulent flow properties, particularly regarding anisotropy, without dramatically increasing computational costs. Adopting such advanced models could significantly enhance the predictive capabilities of CFD simulations, ensuring that the simulations not only reflect more realistic conditions but also boost the overall design and efficiency of FOWTs.

A critical aspect that remains under-assessed is the accurate depiction of the turbulent boundary layer near the bodies of FOWTs in coupled simulations. Typically, a finely detailed grid with a y+ value under 5 is necessary for this. Yet, such refinement results in a high count of mesh cells, escalating computational costs considerably. An alternative approach involves using wall functions with a coarser grid, where y+ values range between 30 and 100, to approximate the turbulent flow within the boundary layer. In many coupled CFD studies of FOWTs, such as those documented in references [24,162,207,208,230], the treatment of the turbulent boundary layer adjacent to the turbines is often unspecified. A significant number of studies bypass the detailed modeling of the turbulent boundary layer near the rotor blades by employing methods like the AL [218]. Furthermore, numerous studies apply wall functions [215,231], and few have achieved boundary layer resolution down to the viscous sublayer using grids with a y+ under 1 [213,232]. Notably, one of the limited investigations assessing the influence of near-wall grid resolution on FOWT CFD simulations was carried out in [110], where the aerodynamic performance of the reference wind turbine (NREL 5 MW) was evaluated with y+ values ranging from 10 to 100. This study utilized the $k - \omega$ SST turbulence model, incorporating wall functions to simulate turbulence effects. The findings revealed that optimal predictions occurred with y+ values around 30, aligning well with the buffer and logarithmic law regions of the boundary layer where wall functions are most effective.

As FOWTs scale up, they encounter increasingly complex atmospheric inflow conditions above the rotor, prominently featuring wind shear where the wind velocity rises

with altitude. While some detailed CFD studies on FOWTs incorporate wind shear effects [139,219], these scenarios are often simplified. Critical aspects like the turbulence characteristics of atmospheric inflow, pivotal to understanding fatigue loads and potential structural failures in turbines, are frequently overlooked. Moreover, the omission of extensive atmospheric turbulence modeling hinders the accurate depiction of wake meandering phenomena, which significantly influence lateral oscillations affecting downstream turbines. The International Electrotechnical Commission (IEC) recommends two turbulence models for simulating atmospheric inflow for wind turbines: the Mann spectral tensor model, and the Kaimal spectral and exponential coherence model [233,234]. Li et al. [235] applied the Kaimal model to study its effects on the aerodynamics of a semi-submersible FOWT, finding that atmospheric turbulence reduced rotor power stability. However, these models, originally designed for smaller, onshore turbines, lack validation for application to larger-scale FOWTs. Doubrawa et al. [236] utilized these models alongside high-fidelity LES to generate atmospheric inflow conditions for spar-buoy FOWTs, observing an overestimation of fatigue loads under high-wind conditions, and underestimation otherwise. Additionally, Nybø et al. [237] highlighted potential inaccuracies in FOWT dynamic response predictions caused by these models. Given these challenges, future research should prioritize enhancing LES methodologies to more accurately simulate atmospheric inflow conditions and extend the validation of the Mann and Kaimal models to better suit large-scale FOWTs, taking into account factors like the atmospheric stability crucial for wake recovery.

In conducting CFD simulations of FOWTs, it is essential to effectively represent both viscous effects and the turbine's detailed geometry to accurately predict the dynamic behaviors of these systems. A significant challenge lies in accurately simulating the ABL, which has a profound impact on the wind loads and the dynamic responses of FOWTs. For improved accuracy in simulations, the LES technique is favored. It typically employs a precursor method where the ABL is initially modeled in a standalone domain devoid of the turbine, creating realistic inflow conditions. These conditions are then applied to a subsequent CFD simulation incorporating the turbine's geometry [238,239]. Additionally, in RANS simulations, maintaining a consistent wind profile as it approaches the turbine is critical. This consistency can be ensured through a strategic mix of boundary settings and the integration of novel source terms within the momentum equations [240–244].

5.2. Aero-Hydro-Elastic Simulations

FOWTs are intricate systems that integrate various components such as wind turbine blades, towers, hubs, nacelles, mooring systems, and floating platforms. The design and development of FOWTs demand interdisciplinary knowledge due to the complex interactions between these components. Despite this complexity, current CFD research into the aero-hydro-elastic performance of FOWTs is limited, often overlooking the critical examination of aeroelastic characteristics. As a result, it is essential to focus more on studying the aero-hydro-elastic behaviors of FOWTs, particularly with respect to large-scale blades and challenging maritime conditions. Incorporating structural models within the aero-hydrodynamic frameworks is vital for addressing blade deformations in FOWTs. The most comprehensive method for aeroelastic analysis involves the use of a three-dimensional (3D) FEM coupled with blade-resolved aerodynamic modeling to capture detailed blade stress and strain accurately. However, this approach faces challenges such as discrepancies between the fluid and structural domain meshes, the necessity for mesh updates due to blade deformations, and elevated computational demands. An alternative method, the 1D equilibrium beam model (EBM), combined with blade-resolved modeling, offers a balanced solution by conserving computational resources. Moreover, the elastic actuator line (EAL) aeroelastic framework presents an efficient strategy by substituting blade-resolved modeling with the AL method and integrating it with the 1D EBM. This approach is particularly effective for reducing the computational overhead in CFD simulations focusing on the aero-hydro-elastic dynamics of FOWTs. Ultimately, the selection of aerodynamic and structural models for an aero-hydro-elastic framework in FOWTs depends on the specific outcomes sought and the computational expenses deemed acceptable.

5.3. Wake Interactions in Multi-FOWT Systems

FOWTs are typically installed in marine wind farms for commercial use. Given the limited sea space and the presence of mooring cables, downstream FOWTs often operate within the wake of upstream turbines, experiencing wake effects. These effects can decrease power output and heighten fatigue loads. Furthermore, floating wind farms tend to face more substantial power reductions due to the low turbulence intensity of high-quality wind resources, compared to their onshore counterparts. Hence, studying the interactions among multiple FOWTs is essential in order to understand the wake dynamics and devise strategies to reduce power losses and fatigue loads in these marine settings. Rezaeiha and Micallef [158] conducted a detailed analysis of wake interactions involving two tandem FOWTs using CFD simulations and the AD method. They examined the effects of three different surge motions of the upstream FOWTs on the power output and wake dynamics between the turbines. Their results showed a modest improvement in average power production from both turbines and an accelerated wake recovery, attributed to enhanced flow mixing caused by the surge movements of the upstream FOWTs. Meanwhile, Zhang et al. [245] explored the dynamics of two FOWTs through blade-resolved modeling, focusing on rotor power, torque, and platform movements. Despite these studies, research on wake interactions among multiple FOWTs remains sparse. For the effective operation of commercial floating wind farms, further in-depth studies on the wake effects across multiple FOWTs are critically needed in order to optimize their performance and durability.

5.4. Simulation of Realistic Sea States

The coupled analyses of FOWTs often focus on regular wave scenarios, examining the system's response under various monochromatic wave conditions. Conversely, simulating realistic, irregular sea states is less frequent, primarily due to the substantial computational resources required. These simulations generally necessitate extended durations, often up to 3 h, to adequately capture all essential nonlinearities and low-frequency dynamics [246]. More recently, however, such simulations have become increasingly prevalent for evaluating the behavior of floaters in authentic marine environments. In these cases, the irregular sea conditions are typically modeled using a low-order approach based on the nonlinear PF theory. The generated sea states are then integrated into a CFD model through a one-way coupling process. This method helps confine the computational domain of the CFD simulations, thereby lessening the overall computational burden [246,247].

6. Conclusions

FOWTs are essential for exploiting offshore wind energy resources. Unlike onshore turbines, floating turbines must operate in a more complex marine environment: the upper section of the turbine experiences wind loads, while the floating base and mooring system withstand the combined effects of waves and ocean currents. These interconnected environmental forces present significant challenges to FOWT design and development. Therefore, accurately predicting the various environmental loads on FOWTs is critically important. This review paper reviewed a thorough evaluation of advancements in CFD related to FOWT design, focusing on the hydrodynamic, aerodynamic, mooring, and structural dynamics. It includes different modeling strategies such as uncoupled to fully coupled approaches.

In wind turbine aerodynamics, the most precise method involves blade-resolved modeling, which captures detailed flow fields on blade surfaces but requires significant computational resources. The parametric modeling of turbine blades, known as actuator models, is more efficient and includes AS, AL, and AD models. The AL-based aeroelastic framework can forecast blade deformations under typical conditions. For a more in-depth analysis, such as evaluating stress and strain in blade structures, blade-resolved modeling using 3D FEM is preferred. Research on streamlined aerodynamics to understand the influence of aerodynamic loads on floating platform dynamics is limited compared to studies employing designated platform motions to explore the unsteady behavior of turbine aerodynamics. Among the six DOF of floating platforms, defined surge and pitch

motions with various frequencies and amplitudes are extensively studied, with the yaw motion examined less frequently. For more realistic conditions, combined wave and wind scenarios are utilized to evaluate the integrated aero-hydrodynamic performance of FOWTs. The structural model is incorporated into the aero-hydrodynamic framework to account for blade deformations of FOWTs. However, detailed CFD simulations of the aero-hydro-elastic behavior of FOWTs are still relatively scarce in research.

Therefore, based on the thorough review conducted in this article, several potential future research directions are suggested to address ongoing challenges in modeling the dynamics of FOWTs:

- Investigate and validate nonlinear EV models for better accuracy in capturing anisotropy in turbulent flows around FOWTs;
- Explore the efficacy of highly refined grid techniques or alternative methods like wall functions to accurately simulate the turbulent boundary layer near FOWT bodies without excessive computational costs;
- Conduct high-fidelity CFD simulations using LES to generate more realistic atmospheric inflow conditions, particularly assessing the effects of large-scale atmospheric turbulence on turbine performance and wake dynamics;
- Assess the impact of different simulation methods for the atmospheric boundary layer on the dynamic responses of FOWTs to ensure an accurate representation of environmental conditions;
- Focus on the integration of aerodynamic, hydrodynamic, and structural dynamics within CFD simulations to address the complex interactions in large-scale FOWTs, especially under severe sea conditions;
- Investigate the physical mechanisms of wake interactions in floating wind farms to optimize the layout and operational strategies, aiming to reduce power deficits and fatigue loads;
- Enhance the simulation models to incorporate realistic, irregular sea states for a better understanding of FOWT behavior under varied wave conditions, which is critical for design and operational planning.

Abbreviations

AD	Actuator disk
AL	Actuator line
AS	Actuator surface
ABL	Atmospheric boundary layer
BEM	Blade element momentum
BEM	Boundary element method
BEMT	Boundary element momentum theory
CFD	Computational fluid dynamics
DOF	Degree of freedom
DNS	Direct numerical simulation
DFBI	Dynamic fluid body interaction
Dyn	Dynamic method
EV	Eddy viscosity
EAL	Elastic actuator line
EBM	Equilibrium beam model
FEM	Finite element method
FVM	Finite volume method
FOWTs	Floating offshore wind turbines
FVW	Free vortex wake method
GDW	Generalized dynamic wake method
HPC	High-performance computing
HAWTs	Horizontal axis wind turbines
IEC	International electrotechnical commission
LES	Large eddy simulation
LCOE	Levelized costs of energy
ME	Morison equation
MIMO	Multi-input multi-output
NREL	National renewable energy laboratory
NSE	Navier–Stokes equations
O&M	Operation and maintenance
PF	Potential flow
QS	Quasi-static method
RTHS	Real-time hybrid simulations
RANS	Reynolds-averaged Navier–Stokes
RST	Reynolds stress turbulence
SST	Shear stress transport
SPM	Single-point mooring
SGS	Subgrid-scale model
SDEs	Stochastic differential equations
TLP	Tension-leg platform
3D	Three-dimensional
TSRs	Tip–speed ratios
ULS	Ultimate limit states
UALM	Unsteady actuator line method
VAWTs	Vertical axis wind turbines
VOF	Volume of fluid
VLM	Vortex lattice method
WECs	Wave energy converters

References

1. Ren, Y.; Shi, W.; Venugopal, V.; Zhang, L.; Li, X. Experimental study of tendon failure analysis for a TLP floating offshore wind turbine. *Appl. Energy* **2024**, *358*, 122633. [CrossRef]
2. Kuriqi, A.; Pinheiro, A.N.; Sordo-Ward, A.; Garrote, L. Flow regime aspects in determining environmental flows and maximising energy production at run-of-river hydropower plants. *Appl. Energy* **2019**, *256*, 113980. [CrossRef]

3. Tian, W.; Wang, Y.; Shi, W.; Michailides, C.; Wan, L.; Chen, M. Numerical study of hydrodynamic responses for a combined concept of semisubmersible wind turbine and different layouts of a wave energy converter. *Ocean Eng.* **2023**, *272*, 113824. [CrossRef]
4. Jiang, Z. Installation of offshore wind turbines: A technical review. *Renew. Sustain. Energy Rev.* **2021**, *139*, 110576. [CrossRef]
5. Wan, L.; Moan, T.; Gao, Z.; Shi, W. A review on the technical development of combined wind and wave energy conversion systems. *Energy* **2024**, *294*, 130885. [CrossRef]
6. Lerch, M.; De-Prada-Gil, M.; Molins, C.; Benveniste, G. Sensitivity analysis on the levelized cost of energy for floating offshore wind farms. *Sustain. Energy Technol.* **2018**, *30*, 77–90. [CrossRef]
7. Wiser, R.; Rand, J.; Seel, J.; Beiter, P.; Baker, E.; Lantz, E.; Gilman, P. Expert elicitation survey predicts 37% to 49% declines in wind energy costs by 2050. *Nat. Energy* **2021**, *6*, 555–565. [CrossRef]
8. Subbulakshmi, A.; Verma, M.; Keerthana, M.; Sasmal, S.; Harikrishna, P.; Kapuria, S. Recent advances in experimental and numerical methods for dynamic analysis of floating offshore wind turbines—An integrated review. *Renew. Sustain. Energy Rev.* **2022**, *164*, 112525. [CrossRef]
9. Bhutta, M.M.A.; Hayat, N.; Farooq, A.U.; Ali, Z.; Jamil, S.R.; Hussain, Z. Vertical axis wind turbine–A review of various configurations and design techniques. *Renew. Sustain. Energy Rev.* **2012**, *16*, 1926–1939. [CrossRef]
10. Möllerström, E.; Gipe, P.; Beurskens, J.; Ottermo, F. A historical review of vertical axis wind turbines rated 100 kW and above. *Renew. Sustain. Energy Rev.* **2019**, *105*, 1–13. [CrossRef]
11. Zhao, Z.; Wang, D.; Wang, T.; Shen, W.; Liu, H.; Chen, M. A review: Approaches for aerodynamic performance improvement of lift-type vertical axis wind turbine. *Sustain. Energy Techn.* **2022**, *49*, 101789. [CrossRef]
12. Matha, D.; Schlipf, M.; Pereira, R.; Jonkman, J. Challenges in simulation of aerodynamics, hydrodynamics, and mooring line dynamics of floating offshore wind turbines. In Proceedings of the ISOPE International Ocean and Polar Engineering Conference, Maui, HI, USA, 19–24 June 2011; p. ISOPE-I.
13. Röckmann, C.; Lagerveld, S.; Stavenuiter, J. Operation and maintenance costs of offshore wind farms and potential multi-use platforms in the Dutch North Sea. *Aquac. Perspect. Multi-Use Sites Open Ocean. Untapped Potential Mar. Resour. Anthr.* **2017**, 97–113. [CrossRef]
14. Gueydon, S.; Bayati, I.; De Ridder, E.J. Discussion of solutions for basin model tests of FOWTs in combined waves and wind. *Ocean Eng.* **2020**, *209*, 107288. [CrossRef]
15. Chen, C.; Ma, Y.; Fan, T. Review of model experimental methods focusing on aerodynamic simulation of floating offshore wind turbines. *Renew. Sustain. Energy Rev.* **2022**, *157*, 112036. [CrossRef]
16. Chen, P.; Chen, J.; Hu, Z. Review of experimental-numerical methodologies and challenges for floating offshore wind turbines. *J. Mar. Sci. Appl.* **2020**, *19*, 339–361. [CrossRef]
17. Wang, X.; Cai, C.; Cai, S.; Wang, T.; Wang, Z.; Song, J.; Rong, X. A review of aerodynamic and wake characteristics of floating offshore wind turbines. *Renew. Sustain. Energy Rev.* **2023**, *175*, 113144. [CrossRef]
18. Basbas, H.; Liu, Y.; Laghrouche, S.; Hilairet, M.; Plestan, F. Review on floating offshore wind turbine models for nonlinear control design. *Energies* **2022**, *15*, 5477. [CrossRef]
19. Faraggiana, E.; Giorgi, G.; Sirigu, M.; Ghigo, A.; Bracco, G.; Mattiazzo, G. A review of numerical modelling and optimisation of the floating support structure for offshore wind turbines. *J. Ocean Eng. Mar. Energy* **2022**, *8*, 433–456. [CrossRef]
20. Zhang, H.; Wang, H.; Cai, X.; Xie, J.; Wang, Y.; Zhang, N. Research on the Dynamic Performance of a Novel Floating Offshore Wind Turbine Considering the Fully-Coupled-Effect of the System. *J. Mar. Sci. Eng.* **2022**, *10*, 341. [CrossRef]
21. Mahmuddin, F. Rotor blade performance analysis with blade element momentum theory. *Energy Procedia* **2017**, *105*, 1123–1129. [CrossRef]
22. Yang, H.; Alkhabbaz, A.; Tongphong, W.; Lee, Y. Cross-comparison analysis of environmental load components in extreme conditions for pontoon-connected semi-submersible FOWT using CFD and potential-based tools. *Ocean Eng.* **2024**, *304*, 117248. [CrossRef]
23. Madsen, H.A.; Bak, C.; Døssing, M.; Mikkelsen, R.; Øye, S. Validation and modification of the blade element momentum theory based on comparisons with actuator disc simulations. *Wind. Energy Int. J. Prog. Appl. Wind. Power Convers. Technol.* **2010**, *13*, 373–389. [CrossRef]
24. Tran, T.T.; Kim, D.H. A CFD study of coupled aerodynamic-hydrodynamic loads on a semisubmersible floating offshore wind turbine. *Wind Energy* **2018**, *21*, 70–85. [CrossRef]
25. Ciuriuc, A.; Rapha, J.I.; Guanche, R.; Domínguez-García, J.L. Digital tools for floating offshore wind turbines (FOWT): A state of the art. *Energy Rep.* **2022**, *8*, 1207–1228. [CrossRef]
26. Otter, A.; Murphy, J.; Pakrashi, V.; Robertson, A.; Desmond, C. A review of modelling techniques for floating offshore wind turbines. *Wind Energy* **2022**, *25*, 831–857. [CrossRef]
27. Micallef, D.; Rezaeiha, A. Floating offshore wind turbine aerodynamics: Trends and future challenges. *Renew. Sustain. Energy Rev.* **2021**, *152*, 111696. [CrossRef]
28. Didier, F.; Liu, Y.; Laghrouche, S.; Depernet, D. A Comprehensive Review on Advanced Control Methods for Floating Offshore Wind Turbine Systems above the Rated Wind Speed. *Energies* **2024**, *17*, 2257. [CrossRef]
29. Edwards, E.C.; Holcombe, A.; Brown, S.; Ransley, E.; Hann, M.; Greaves, D. Trends in floating offshore wind platforms: A review of early-stage devices. *Renew. Sustain. Energy Rev.* **2024**, *193*, 114271. [CrossRef]

30. Shi, W.; Fu, J.; Ren, Z.; Jiang, Z.; Wang, T.; Cui, L.; Li, X. Real-time hybrid model tests of floating offshore wind turbines: Status, challenges, and future trends. *Appl. Ocean Res.* **2023**, *141*, 103796. [CrossRef]

31. Ojo, A.; Collu, M.; Coraddu, A. Multidisciplinary design analysis and optimization of floating offshore wind turbine substructures: A review. *Ocean Eng.* **2022**, *266*, 112727. [CrossRef]

32. Xu, S.; Xue, Y.; Zhao, W.; Wan, D. A review of high-fidelity computational fluid dynamics for floating offshore wind turbines. *J. Mar. Sci. Eng.* **2022**, *10*, 1357. [CrossRef]

33. Zhang, W.; Calderon-Sanchez, J.; Duque, D.; Souto-Iglesias, A. Computational Fluid Dynamics (CFD) applications in Floating Offshore Wind Turbine (FOWT) dynamics: A review. *Appl. Ocean Res.* **2024**, *150*, 104075. [CrossRef]

34. Liu, Y. A CFD Study of Fluid-Structure Interaction Problems for Floating Offshore Wind Turbines. Ph.D. Thesis, University of Strathclyde, Glasgow, Scotland, 2018.

35. Musial, W. Overview of Floating Offshore Wind. In Proceedings of the Webinar Hosted by National Renewable Energy Laboratory, Golden, CO, USA, 26 February 2020.

36. Wang, L.; Liu, X.; Kolios, A. State of the art in the aeroelasticity of wind turbine blades: Aeroelastic modelling. *Renew. Sustain. Energy Rev.* **2016**, *64*, 195–210. [CrossRef]

37. Cordle, A.; Jonkman, J. State of the Art in FloatingWind Turbine Design Tools. In Proceedings of the Twenty-First International Offshore and Polar Engineering Conference, Maui, HI, USA, 19–24 June 2011; Available online: https://www.onepetro.org/conference-paper/ISOPE-I-11-112 (accessed on 12 June 2024).

38. Lemmer, F.; Yu, W.; Luhmann, B.; Schlipf, D.; Cheng, P.W. Multibody modeling for concept-level floating offshore wind turbine design. *Multibody Syst. Dyn.* **2020**, *49*, 203–236. [CrossRef]

39. Nguyen, M.T.; Dang, T.D.; Ahn, K.K. Application of electro-hydraulic actuator system to control continuously variable transmission in wind energy converter. *Energies* **2019**, *12*, 2499. [CrossRef]

40. Yin, X.; Lin, Y.; Li, W.; Gu, H. Hydro-viscous transmission based maximum power extraction control for continuously variable speed wind turbine with enhanced efficiency. *Renew. Energy* **2016**, *87*, 646–655. [CrossRef]

41. Yin, X.; Lin, Y.; Li, W.; Liu, H.; Gu, Y. Output power control for hydro-viscous transmission based continuously variable speed wind turbine. *Renew. Energy* **2014**, *72*, 395–405. [CrossRef]

42. Kumar, D.; Chatterjee, K. A review of conventional and advanced MPPT algorithms for wind energy systems. *Renew. Sustain. Energy Rev.* **2016**, *55*, 957–970. [CrossRef]

43. Chiang, M. A novel pitch control system for a wind turbine driven by a variable-speed pump-controlled hydraulic servo system. *Mechatronics* **2011**, *21*, 753–761. [CrossRef]

44. Yin, X.; Lin, Y.; Li, W. Predictive pitch control of an electro-hydraulic digital pitch system for wind turbines based on the extreme learning machine. *Trans. Inst. Meas. Control.* **2016**, *38*, 1392–1400. [CrossRef]

45. Verma, M.; Nartu, M.K.; Subbulakshmi, A. Optimal TMD design for floating offshore wind turbines considering model uncertainties and physical constraints. *Ocean Eng.* **2022**, *243*, 110236. [CrossRef]

46. He, E.M.; Hu, Y.Q.; Zhang, Y. Optimization design of tuned mass damper for vibration suppression of a barge-type offshore floating wind turbine. *Proc. Inst. Mech. Eng. Part M J. Eng. Marit. Environ.* **2017**, *231*, 302–315. [CrossRef]

47. Brodersen, M.L.; Bjørke, A.S.; Høgsberg, J. Active tuned mass damper for damping of offshore wind turbine vibrations. *Wind Energy* **2017**, *20*, 783–796. [CrossRef]

48. Ghassempour, M.; Failla, G.; Arena, F. Vibration mitigation in offshore wind turbines via tuned mass damper. *Eng. Struct.* **2019**, *183*, 610–636. [CrossRef]

49. Jaksic, V.; Wright, C.S.; Murphy, J.; Afeef, C.; Ali, S.F.; Mandic, D.P.; Pakrashi, V. Dynamic response mitigation of floating wind turbine platforms using tuned liquid column dampers. *Philos. Trans. R. Soc. A Math. Phys. Eng. Sci.* **2015**, *373*, 20140079. [CrossRef]

50. Subbulakshmi, A.; Sundaravadivelu, R. Effects of damping plate position on heave and pitch responses of spar platform with single and double damping plates under regular waves. *Ocean Eng.* **2021**, *224*, 108719. [CrossRef]

51. Subbulakshmi, A.; Sundaravadivelu, R. Heave damping of spar platform for offshore wind turbine with heave plate. *Ocean Eng.* **2016**, *121*, 24–36. [CrossRef]

52. El Beshbichi, O.; Xing, Y.; Chen Ong, M. Linear quadratic regulator optimal control of two-rotor wind turbine mounted on spar-type floating platform. *J. Offshore Mech. Arct. Eng.* **2023**, *145*, 022001. [CrossRef]

53. Li, S.; Han, Y.; Pan, W.; Liu, S.; Hou, M. Variable-gain higher-order sliding mode pitch control of floating offshore wind turbine. *J. Mar. Sci. Eng.* **2021**, *9*, 1172. [CrossRef]

54. Allison, J.T.; Zalkind, D.S.; Herber, D.R. Open-Loop Control Co-Design of Semisubmersible Floating Offshore Wind Turbines Using Linear Parameter-Varying Models. *J. Mech. Design* **2024**, *146*, 041704-1.

55. Jard, T.; Snaiki, R. Real-time repositioning of floating wind turbines using model predictive control for position and power regulation. *Wind* **2023**, *3*, 131–150. [CrossRef]

56. Song, Y.; Jeon, T.; Paek, I.; Dugarjav, B. Design and Validation of Pitch H-Infinity Controller for a Large Wind Turbine. *Energies* **2022**, *15*, 8763. [CrossRef]

57. Brunton, S.L.; Noack, B.R. Closed-loop turbulence control: Progress and challenges. *Appl. Mech. Rev.* **2015**, *67*, 050801. [CrossRef]

58. Society for Underwater Technology. South West–Offshore Floating Wind–Design and Installation. Available online: https://www.sut.org/event/south-west-offshore-floating-wind-design-and-installation/ (accessed on 1 July 2024).

59. James, R.; Weng, W.Y.; Spradbery, C.; Jones, J.; Matha, D.; Mitzlaff, A.; Ahilan, R.; Frampton, M.; Lopes, M. Floating Wind Joint Industry Project—Phase I Summary Report. *Carbon Trust Technol. Rep.* **2018**, *19*, 2–20.

60. Kim, D.; Bae, Y.H.; Park, S. Design strategy for resonance avoidance to improve the performance of tension leg platform-type floating offshore wind turbines. *Ocean Eng.* **2024**, *306*, 118080. [CrossRef]

61. Zhai, Y.; Zhao, H.; Li, X.; Shi, W. Design and Dynamic Analysis of a Novel Large-Scale Barge-Type Floating Offshore Wind Turbine with Aquaculture Cage. *J. Mar. Sci. Eng.* **2022**, *10*, 1926. [CrossRef]

62. Thiagarajan, K.P.; Dagher, H.J. A review of floating platform concepts for offshore wind energy generation. *J. Offshore Mech. Arct. Eng.* **2014**, *136*, 020903. [CrossRef]

63. Liu, Y.; Yoshida, S.; Yamamoto, H.; Toyofuku, A.; He, G.; Yang, S. Response characteristics of the DeepCwind floating wind turbine moored by a single-point mooring system. *Appl. Sci.* **2018**, *8*, 2306. [CrossRef]

64. Nihei, Y.; Matsuda, Y.; Kitamura, S.; Takaiwa, K.; Kanda, N. Research and development about the mechanisms of a single point mooring system for offshore wind turbines. *Ocean Eng.* **2018**, *147*, 431–446. [CrossRef]

65. Zhong, W.; Zhao, W.; Wan, D.; Zhao, Y. Comparison study on mooring line models for hydrodynamic performances of floating offshore wind turbines. *Ocean Eng.* **2024**, *296*, 117083. [CrossRef]

66. Masciola, M.; Jonkman, J.; Robertson, A. Implementation of a Multisegmented, Quasi-Static Cable Model. In Proceedings of the 23rd International Offshore and Polar Engineering Conference, Anchorage, AK, USA, 30 June–5 July 2013.

67. Cevasco, D.; Collu, M.; Rizzo, C.M.; Hall, M. On mooring line tension and fatigue prediction for offshore vertical axis wind turbines: A comparison of lumped mass and quasi-static approaches. *Wind Eng.* **2018**, *42*, 97–107. [CrossRef]

68. Ishihara, T.; Phuc, P.V.; Sukegawa, H.; Shimada, K. A study on the dynamic response of a semi-submersible floating offshore wind turbine system Part 1: A water tank test. In Proceedings of the 12th International Conference on Wind Engineering: ICWE 12, Cairns, Australia, 1–6 July 2007; p. 4.

69. Hall, M.; Buckham, B.; Crawford, C. Evaluating the importance of mooring line model fidelity in floating offshore wind turbine simulations. *Wind Energy* **2014**, *17*, 1835–1853. [CrossRef]

70. Azcona, J.; Nygaard, T.A.; Munduate, X.; Merino, D. *Development of a Code for Dynamic Simulation of Mooring Lines in Contact with Seabed*; EWEA Offshore: Amsterdam, The Netherlands, 2011.

71. Palm, J.; Eskilsson, C.; Bergdahl, L. An hp-adaptive discontinuous Galerkin method for modelling snap loads in mooring cables. *Ocean Eng.* **2017**, *144*, 266–276. [CrossRef]

72. Palm, J.; Eskilsson, C.; Paredes, G.M.; Bergdahl, L. Coupled mooring analysis for floating wave energy converters using CFD: Formulation and validation. *Int. J. Mar. Energy* **2016**, *16*, 83–99. [CrossRef]

73. Müller, K.; Lemmer, F.; Borisade, F.; Kretschmer, M.; Gruber, J.; Hagemann, L. State-of-the-art FOWT design practice and guidelines. *Lifes50+ Deliv.* **2016**, *7*, 2016.

74. Larsen, T.J.; Hansen, A.M. *How 2 HAWC2, the User's Manual*; Risø National Laboratory: Roskilde, Denmark, 2007.

75. Jonkman, J.M. *FAST User's Guide*; National Renewable Energy Laboratory: Golden, CO, USA, 2005; Volume 365.

76. DNV GL. *Coupled Analysis of Floating Wind Turbines*; DNVGL-RP-0286; DNV GL: Høvik, Norway, 2019.

77. Wood, D.H.; Golmirzaee, N. A revision of blade element/momentum theory for wind turbines in their high-thrust region. *Front. Energy Res.* **2023**, *11*, 1256308. [CrossRef]

78. Faltinsen, O. *Sea Loads on Ships and Offshore Structures*; Cambridge University Press: Cambridge, UK, 1993; Volume 1.

79. Xu, B.F.; Wang, T.G.; Yuan, Y.; Zhao, Z.Z.; Liu, H.M. A simplified free vortex wake model of wind turbines for axial steady conditions. *Appl. Sci.* **2018**, *8*, 866. [CrossRef]

80. Jiang, Z.; Xing, Y.; Guo, Y.; Moan, T.; Gao, Z. Long-term contact fatigue analysis of a planetary bearing in a land-based wind turbine drivetrain. *Wind Energy* **2015**, *18*, 591–611. [CrossRef]

81. Zienkiewicz, O.C.; Taylor, R.L.; Zhu, J.Z. *The Finite Element Method: Its Basis and Fundamental*; Elsevier: Amsterdam, The Netherlands, 2005.

82. Li, C.B.; Chen, M.; Choung, J. The quasi-static response of moored floating structures based on minimization of mechanical energy. *J. Mar. Sci. Eng.* **2021**, *9*, 960. [CrossRef]

83. Dong, Y.; Chen, Y.; Liu, H.; Zhou, S.; Ni, Y.; Cai, C.; Zhou, T.; Li, Q. Review of Study on the Coupled Dynamic Performance of Floating Offshore Wind Turbines. *Energies* **2022**, *15*, 3970. [CrossRef]

84. Morison, J.R.; Johnson, J.W.; Schaaf, S.A. The force exerted by surface waves on piles. *J. Pet. Technol.* **1950**, *2*, 149–154. [CrossRef]

85. Brebbia, C.A. *The Boundary Element Method for Engineers*; Pentech Press: Xi'an, China, 1978.

86. Tu, J.; Yeoh, G.H.; Liu, C. *Computational Fluid Dynamics: A Practical Approach*; Butterworth-Heinemann: Oxford, UK, 2018.

87. Orcina Ltd. *OrcaFlex*, Version 10.3d; Orcina Ltd.: Ulverston, UK, 2019.

88. *Flexcom Technical Manual*; Wood Group Kenny: Galway, Ireland, 2014.

89. Systèmes, D. Simpack MBS Software | Dassault Systèmes. Available online: https://www.3ds.com/products/simulia/simpack (accessed on 1 July 2024).

90. Marine Operations and Mooring Analysis Software—Sima. Available online: https://www.dnv.com/services/marine-operations-and-mooring-analysis-software-sima-2324/ (accessed on 1 July 2024).

91. Jasak, H. OpenFOAM: Open source CFD in research and industry. *Int. J. Nav. Archit. Ocean Eng.* **2009**, *1*, 89–94.

92. Ansys. Ansys | Engineering Simulation Software. Available online: https://www.ansys.com (accessed on 1 July 2024).

93. Hibbitt, Karlsson & Sorensen, Inc. *ABAQUS/Standard User's Manual*; ABAQUS; Hibbitt, Karlsson & Sorensen, Inc.: Pawtucket, RI, USA, 2010.

94. Simcenter Star-CCM+ Documentation, Version 2020.2. 2020. Available online: https://www.aerofem.com/assets/files/Simcenter-STAR-CCM-2020.2-New-FeaturesFact-Sheet.pdf (accessed on 1 July 2024).

95. Shen, C.; Chen, N. A SWENSE-based wave-induced loading simulation for a semi-submersible FOWT platform. *Ocean Eng.* **2024**, *311*, 118950. [CrossRef]

96. Archambeau, F.; Méchitoua, N.; Sakiz, M. Code Saturne: A finite volume code for the computation of turbulent incompressible flows-Industrial applications. *Int. J. Finite Vol.* **2004**, *1*, 1–62.

97. Bihs, H.; Kamath, A.; Alagan Chella, M.; Aggarwal, A.; Arntsen, Ø.A. A new level set numerical wave tank with improved density interpolation for complex wave hydrodynamics. *Comput. Fluids* **2016**, *140*, 191–208. [CrossRef]

98. Benitz, M.A.; Lackner, M.A.; Schmidt, D.P. Hydrodynamics of offshore structures with specific focus on wind energy applications. *Renew. Sustain. Energy Rev.* **2015**, *44*, 692–716. [CrossRef]

99. Edition, F.; Journée, J.; Massie, W.W. *Offshore Hydromechanics*; Delft Univ. Technology: Delft, The Netherlands, 2001.

100. Uzunoglu, E.; Soares, C.G. On the model uncertainty of wave induced platform motions and mooring loads of a semisubmersible based wind turbine. *Ocean Eng.* **2018**, *148*, 277–285. [CrossRef]

101. Leble, V.; Barakos, G. Demonstration of a coupled floating offshore wind turbine analysis with high-fidelity methods. *J. Fluid. Struct.* **2016**, *62*, 272–293. [CrossRef]

102. Siddiqui, M.A.; Hanssen, F.W.; Greco, M.; Anda, E. Comparing the Utility of Coupled Aero-Hydrodynamic Analysis Using a CFD Solver versus a Potential Flow Solver for Floating Offshore Wind Turbines. *Energies* **2023**, *16*, 7833. [CrossRef]

103. Zhou, Y.; Xiao, Q.; Liu, Y.; Incecik, A.; Peyrard, C.; Li, S.; Pan, G. Numerical modelling of dynamic responses of a floating offshore wind turbine subject to focused waves. *Energies* **2019**, *12*, 3482. [CrossRef]

104. Liu, Y.; Xiao, Q.; Incecik, A.; Wan, D. Investigation of the effects of platform motion on the aerodynamics of a floating offshore wind turbine. *J. Hydrodyn.* **2016**, *28*, 95–101. [CrossRef]

105. Lee, H.; Lee, D. Effects of platform motions on aerodynamic performance and unsteady wake evolution of a floating offshore wind turbine. *Renew. Energy* **2019**, *143*, 9–23. [CrossRef]

106. Schulz, C.W.; Netzband, S.; Özinan, U.; Cheng, P.W.; Abdel-Maksoud, M. Wind turbine rotors in surge motion: New insights into unsteady aerodynamics of floating offshore wind turbines (FOWTs) from experiments and simulations. *Wind Energy Sci.* **2024**, *9*, 665–695. [CrossRef]

107. Schulz, C.W.; Netzband, S.; Özinan, U.; Cheng, P.W.; Abdel-Maksoud, M. Wind turbine rotors in surge motion: New insights into unsteady aerodynamics of FOWT from experiments and simulations. *Wind. Energy Sci. Discuss.* **2023**, *2023*, 1–47.

108. Henriksen, L.C.; Hansen, M.H.; Poulsen, N.K. A simplified dynamic inflow model and its effect on the performance of free mean wind speed estimation. *Wind Energy* **2013**, *16*, 1213–1224. [CrossRef]

109. Ferreira, C.; Yu, W.; Sala, A.; Viré, A. Dynamic inflow model for a floating horizontal axis wind turbine in surge motion. *Wind Energy Sci.* **2022**, *7*, 469–485. [CrossRef]

110. Wu, C.H.K.; Nguyen, V.T. Aerodynamic simulations of offshore floating wind turbine in platform-induced pitching motion. *Wind Energy* **2017**, *20*, 835–858. [CrossRef]

111. Liu, Y.; Xiao, Q.; Incecik, A.; Peyrard, C. Aeroelastic analysis of a floating offshore wind turbine in platform-induced surge motion using a fully coupled CFD-MBD method. *Wind Energy* **2019**, *22*, 1–20. [CrossRef]

112. Ramos García, N.; Kontos, S.; Pegalajar Jurado, A.; González Horcas, S.; Bredmose, H. Investigation of the floating IEA Wind 15 MW RWT using vortex methods Part I: Flow regimes and wake recovery. *Wind Energy* **2022**, *25*, 468–504. [CrossRef]

113. Sebastian, T.; Lackner, M.A. Development of a free vortex wake method code for offshore floating wind turbines. *Renew. Energy* **2012**, *46*, 269–275. [CrossRef]

114. Shaler, K.; Branlard, E.; Platt, A.; Jonkman, J. Preliminary introduction of a free vortex wake method into OpenFAST. *J. Phys. Conf. Ser.* **2020**, *1452*, 012064. [CrossRef]

115. Sebastian, T.; Lackner, M. Analysis of the induction and wake evolution of an offshore floating wind turbine. *Energies* **2012**, *5*, 968–1000. [CrossRef]

116. Kadum, H.; Rockel, S.; Viggiano, B.; Dib, T.; Hölling, M.; Chevillard, L.; Cal, R.B. Assessing intermittency characteristics via cumulant analysis of floating wind turbines wakes. *J. Renew. Sustain. Energy* **2021**, *13*, 013302. [CrossRef]

117. Tran, T.; Kim, D. The platform pitching motion of floating offshore wind turbine: A preliminary unsteady aerodynamic analysis. *J. Wind Eng. Ind. Aerod.* **2015**, *142*, 65–81. [CrossRef]

118. Rega, G. Nonlinear vibrations of suspended cables—Part II: Deterministic phenomena. *Appl. Mech. Rev.* **2004**, *57*, 479–514. [CrossRef]

119. Larsen, J.W.; Nielsen, S.R. Non-linear dynamics of wind turbine wings. *Int. J. Nonlin. Mech.* **2006**, *41*, 629–643. [CrossRef]

120. Larsen, J.W.; Nielsen, S.R. Nonlinear parametric instability of wind turbine wings. *J. Sound Vib.* **2007**, *299*, 64–82. [CrossRef]

121. Jaksic, V.; O'Shea, R.; Cahill, P.; Murphy, J.; Mandic, D.P.; Pakrashi, V. Dynamic response signatures of a scaled model platform for floating wind turbines in an ocean wave basin. *Philos. Trans. R. Soc. A Math. Phys. Eng. Sci.* **2015**, *373*, 20140078. [CrossRef]

122. Campos, A.; Molins, C.; Trubat, P.; Alarcón, D. A 3D FEM model for floating wind turbines support structures. *Energy Procedia* **2017**, *137*, 177–185. [CrossRef]

123. Sun, C. Mitigation of offshore wind turbine responses under wind and wave loading: Considering soil effects and damage. *Struct. Control. Health Monit.* **2018**, *25*, e2117. [CrossRef]

124. Tagliafierro, B.; Karimirad, M.; Altomare, C.; Göteman, M.; Martínez-Estévez, I.; Capasso, S.; Domínguez, J.M.; Viccione, G.; Gómez-Gesteira, M.; Crespo, A.J. Numerical validations and investigation of a semi-submersible floating offshore wind turbine platform interacting with ocean waves using an SPH framework. *Appl. Ocean Res.* **2023**, *141*, 103757. [CrossRef]

125. Meier, C.; Popp, A.; Wall, W.A. Geometrically exact finite element formulations for slender beams: Kirchhoff–Love theory versus Simo–Reissner theory. *Arch. Comput. Method E* **2019**, *26*, 163–243. [CrossRef]

126. Bathe, K.J. *Finite Element Procedures*; Prentice Hall: Upper Saddle River, NJ, USA, 1996.

127. Farhat, C.; Avery, P.; Chapman, T.; Cortial, J. Dimensional reduction of nonlinear finite element dynamic models with finite rotations and energy-based mesh sampling and weighting for computational efficiency. *Int. J. Numer. Meth. Eng.* **2014**, *98*, 625–662. [CrossRef]

128. Oh, S.; Ishii, K.; Iijima, K.; Suzuki, H. Implementation of potential flow hydrodynamics to time-domain analysis of flexible platforms of floating offshore wind turbines. *J. Phys. Conf. Ser.* **2019**, *1356*, 012041. [CrossRef]

129. Cheng, A.H.; Cheng, D.T. Heritage and early history of the boundary element method. *Eng. Anal. Bound Elem.* **2005**, *29*, 268–302. [CrossRef]

130. Atcheson, M.; Garrad, A.; Cradden, L.; Henderson, A.; Matha, D.; Nichols, J.; Roddier, D.; Sandberg, J. *Floating Offshore Wind Energy*; Springer: Berlin/Heidelberg, Germany, 2016; Volume 10, pp. 978–983.

131. Suzuki, H.; Shiohara, H.; Schnepf, A.; Houtani, H.; Carmo, L.H.; Hirabayashi, S.; Haneda, K.; Chujo, T.; Nihei, Y.; Malta, E.B. Wave and wind responses of a very-light fowt with guy-wired-supported tower: Numerical and experimental studies. *J. Mar. Sci. Eng.* **2020**, *8*, 841. [CrossRef]

132. Freyer, K. Wire Ropes Under Bending and Tensile Stresses. In *Wire Ropes*; Springer: Berlin/Heidelberg, Germany, 2007.

133. Cardiff, P.; Demirdžić, I. Thirty years of the finite volume method for solid mechanics. *Arch Comput. Method E* **2021**, *28*, 3721–3780. [CrossRef]

134. Yang, S.; Ringsberg, J.W.; Johnson, E.; Hu, Z. Biofouling on mooring lines and power cables used in wave energy converter systems—Analysis of fatigue life and energy performance. *Appl. Ocean Res.* **2017**, *65*, 166–177. [CrossRef]

135. Qiao, D.; Haider, R.; Yan, J.; Ning, D.; Li, B. Review of wave energy converter and design of mooring system. *Sustainability* **2020**, *12*, 8251. [CrossRef]

136. Azcona, J.; Palacio, D.; Munduate, X.; Gonzalez, L.; Nygaard, T.A. Impact of mooring lines dynamics on the fatigue and ultimate loads of three offshore floating wind turbines computed with IEC 61400-3 guideline. *Wind Energy* **2017**, *20*, 797–813. [CrossRef]

137. Chen, L.; Basu, B.; Nielsen, S.R. Nonlinear periodic response analysis of mooring cables using harmonic balance method. *J. Sound Vib.* **2019**, *438*, 402–418. [CrossRef]

138. Ishihara, T.; Zhang, S. Prediction of dynamic response of semi-submersible floating offshore wind turbine using augmented Morison's equation with frequency dependent hydrodynamic coefficients. *Renew. Energy* **2019**, *131*, 1186–1207. [CrossRef]

139. Zhou, Y.; Xiao, Q.; Liu, Y.; Incecik, A.; Peyrard, C.; Wan, D.; Pan, G.; Li, S. Exploring inflow wind condition on floating offshore wind turbine aerodynamic characterisation and platform motion prediction using blade resolved CFD simulation. *Renew. Energy* **2022**, *182*, 1060–1079. [CrossRef]

140. Cao, J.; Qin, Z.; Ju, Y.; Chen, Y.; Shen, W.Z.; Shen, X.; Ke, S. Study of air compressibility effects on the aerodynamic performance of the IEA-15 MW offshore wind turbine. *Energy Convers. Manag.* **2023**, *282*, 116883. [CrossRef]

141. Fang, Y.; Duan, L.; Han, Z.; Zhao, Y.; Yang, H. Numerical analysis of aerodynamic performance of a floating offshore wind turbine under pitch motion. *Energy* **2020**, *192*, 116621. [CrossRef]

142. Sanderse, B.; Van der Pijl, S.P.; Koren, B. Review of computational fluid dynamics for wind turbine wake aerodynamics. *Wind Energy* **2011**, *14*, 799–819. [CrossRef]

143. Thé, J.; Yu, H. A critical review on the simulations of wind turbine aerodynamics focusing on hybrid RANS-LES methods. *Energy* **2017**, *138*, 257–289. [CrossRef]

144. Abkar, M. Impact of subgrid-scale modeling in actuator-line based large-eddy simulation of vertical-axis wind turbine wakes. *Atmosphere* **2018**, *9*, 257. [CrossRef]

145. Leonard, A. Energy cascade in large-eddy simulations of turbulent fluid flow. *Adv. Geophys.* **1974**, *18*, 237–248.

146. Wu, C.; Wang, Q.; Yuan, R.; Luo, K.; Fan, J. Large eddy simulation of the layout effects on wind farm performance coupling with wind turbine control strategies. *J. Energy Resour. Technol.* **2022**, *144*, 051304. [CrossRef]

147. Porté-Agel, F.; Meneveau, C.; Parlange, M.B. A scale-dependent dynamic model for large-eddy simulation: Application to a neutral atmospheric boundary layer. *J. Fluid. Mech.* **2000**, *415*, 261–284. [CrossRef]

148. Abdulqadir, S.A.; Iacovides, H.; Nasser, A. The physical modelling and aerodynamics of turbulent flows around horizontal axis wind turbines. *Energy* **2017**, *119*, 767–799. [CrossRef]

149. Abkar, M.; Moin, P. Large-eddy simulation of thermally stratified atmospheric boundary-layer flow using a minimum dissipation model. *Bound-Lay Meteorol.* **2017**, *165*, 405–419. [CrossRef]

150. Sørensen, J.N.; Mikkelsen, R.F.; Henningson, D.S.; Ivanell, S.; Sarmast, S.; Andersen, S.J. Simulation of wind turbine wakes using the actuator line technique. *Philos. Trans. R. Soc. A Math. Phys. Eng. Sci.* **2015**, *373*, 20140071. [CrossRef]

151. Amiri, M.M.; Shadman, M.; Estefen, S.F. A review of physical and numerical modeling techniques for horizontal-axis wind turbine wakes. *Renew. Sustain. Energy Rev.* **2024**, *193*, 114279. [CrossRef]

152. Whale, J.; Anderson, C.G.; Bareiss, R.; Wagner, S. An experimental and numerical study of the vortex structure in the wake of a wind turbine. *J. Wind Eng. Ind. Aerod.* **2000**, *84*, 1–21. [CrossRef]

153. Ivanell, S.; Sørensen, J.N.; Mikkelsen, R.; Henningson, D. Analysis of numerically generated wake structures. *Wind Energy* **2009**, *12*, 63–80. [CrossRef]

154. Mejia, O.D.L.; Quiñones, J.J.; Laín, S. RANS and hybrid RANS-LES simulations of an H-type Darrieus vertical axis water turbine. *Energies* **2018**, *11*, 2348. [CrossRef]

155. Lei, H.; Zhou, D.; Bao, Y.; Chen, C.; Ma, N.; Han, Z. Numerical simulations of the unsteady aerodynamics of a floating vertical axis wind turbine in surge motion. *Energy* **2017**, *127*, 1–17. [CrossRef]

156. Heinz, S. A review of hybrid RANS-LES methods for turbulent flows: Concepts and applications. *Prog. Aerosp. Sci.* **2020**, *114*, 100597. [CrossRef]

157. Syawitri, T.P.; Yao, Y.F.; Chandra, B.; Yao, J. Comparison study of URANS and hybrid RANS-LES models on predicting vertical axis wind turbine performance at low, medium and high tip speed ratio ranges. *Renew. Energy* **2021**, *168*, 247–269. [CrossRef]

158. Xu, S.; Yang, X.; Zhao, W.; Wan, D. Numerical analysis of aero-hydrodynamic wake flows of a floating offshore wind turbine subjected to atmospheric turbulence inflows. *Ocean Eng.* **2024**, *300*, 117498. [CrossRef]

159. Bai, C.; Wang, W. Review of computational and experimental approaches to analysis of aerodynamic performance in horizontal-axis wind turbines (HAWTs). *Renew. Sustain. Energy Rev.* **2016**, *63*, 506–519. [CrossRef]

160. Tran, T.T.; Kim, D. The coupled dynamic response computation for a semi-submersible platform of floating offshore wind turbine. *J. Wind Eng. Ind. Aerod.* **2015**, *147*, 104–119. [CrossRef]

161. Burmester, S.; Vaz, G.; Gueydon, S.; El Moctar, O. Investigation of a semi-submersible floating wind turbine in surge decay using CFD. *Ship Technol. Res.* **2020**, *67*, 2–14. [CrossRef]

162. Zhao, W.; Wan, D. Numerical study of interactions between phase II of OC4 wind turbine and its semi-submersible floating support system. *J. Ocean Wind Energy* **2015**, *2*, 45–53.

163. Bruinsma, N.; Paulsen, B.T.; Jacobsen, N.G. Validation and application of a fully nonlinear numerical wave tank for simulating floating offshore wind turbines. *Ocean Eng.* **2018**, *147*, 647–658. [CrossRef]

164. Boussinesq, J. Theorie de l'ecoulement tourbillant. *Mem. Acad. Sci.* **1877**, *23*, 46.

165. Ammara, I.; Leclerc, C.; Masson, C. A viscous three-dimensional differential/actuator-disk method for the aerodynamic analysis of wind farms. *J. Sol. Energy* **2002**, *124*, 345–356. [CrossRef]

166. Eça, L.; Hoekstra, M. Near-wall profiles of mean flow and turbulence quantities predicted by eddy-viscosity turbulence models. *Int. J. Numer. Methods Fluids* **2010**, *63*, 953–988. [CrossRef]

167. Swanson, R.C.; Rossow, C. An efficient solver for the RANS equations and a one-equation turbulence model. *Comput. Fluids* **2011**, *42*, 13–25. [CrossRef]

168. Heinz, S.; Mokhtarpoor, R.; Stoellinger, M. Theory-based Reynolds-averaged Navier–Stokes equations with large eddy simulation capability for separated turbulent flow simulations. *Phys. Fluids* **2020**, *32*, 065102. [CrossRef]

169. Burmester, S.; Vaz, G.; El Moctar, O. Towards credible CFD simulations for floating offshore wind turbines. *Ocean Eng.* **2020**, *209*, 107237. [CrossRef]

170. Li, H.; Bachynski-Polić, E.E. Analysis of difference-frequency wave loads and quadratic transfer functions on a restrained semi-submersible floating wind turbine. *Ocean Eng.* **2021**, *232*, 109165. [CrossRef]

171. Pinto, M.L.; Franzini, G.R.; Simos, A.N. A CFD analysis of NREL's 5MW wind turbine in full and model scales. *J. Ocean Eng. Mar. Energy* **2020**, *6*, 211–220. [CrossRef]

172. Naderi, S.; Parvanehmasiha, S.; Torabi, F. Modeling of horizontal axis wind turbine wakes in Horns Rev offshore wind farm using an improved actuator disc model coupled with computational fluid dynamic. *Energy Convers. Manag.* **2018**, *171*, 953–968. [CrossRef]

173. Rezaeiha, A.; Micallef, D. Wake interactions of two tandem floating offshore wind turbines: CFD analysis using actuator disc model. *Renew. Energy* **2021**, *179*, 859–876. [CrossRef]

174. O'Brien, J.M.; Young, T.M.; Early, J.M.; Griffin, P.C. An assessment of commercial CFD turbulence models for near wake HAWT modelling. *J. Wind Eng. Ind. Aerod.* **2018**, *176*, 32–53. [CrossRef]

175. Vogel, C.R.; Willden, R.H. Investigation of wind turbine wake superposition models using Reynolds-averaged Navier-Stokes simulations. *Wind Energy* **2020**, *23*, 593–607. [CrossRef]

176. Amiri, M.M.; Shadman, M.; Estefen, S.F. URANS simulations of a horizontal axis wind turbine under stall condition using Reynolds stress turbulence models. *Energy* **2020**, *213*, 118766. [CrossRef]

177. Antonini, E.G.; Romero, D.A.; Amon, C.H. Improving CFD wind farm simulations incorporating wind direction uncertainty. *Renew. Energy* **2019**, *133*, 1011–1023. [CrossRef]

178. Schumann, U. Realizability of Reynolds-stress turbulence models. *Phys. Fluids* **1977**, *20*, 721–725. [CrossRef]

179. Cabezon, D.; Migoya, E.; Crespo, A. Comparison of turbulence models for the computational fluid dynamics simulation of wind turbine wakes in the atmospheric boundary layer. *Wind Energy* **2011**, *14*, 909–921. [CrossRef]

180. Gomez-Elvira, R.; Crespo, A.; Migoya, E.; Manuel, F.; Hernández, J. Anisotropy of turbulence in wind turbine wakes. *J. Wind Eng. Ind. Aerod.* **2005**, *93*, 797–814. [CrossRef]

181. Yang, X.; Sotiropoulos, F. On the predictive capabilities of LES-actuator disk model in simulating turbulence past wind turbines and farms. In Proceedings of the 2013 American Control Conference, Washington, DC, USA, 17–19 June 2013; pp. 2878–2883.

182. Corniglion, R.; Harris, J.; Peyrard, C.; Capaldo, M. In Comparison of the free vortex wake and actuator line methods to study the loads of a wind turbine in imposed surge motion. *J. Phys. Conf. Ser.* **2020**, *1618*, 052045. [CrossRef]

183. Sanvito, A.G.; Persico, G.; Schito, P.; Dossena, V.; Zasso, A. In Comparative assessment of actuator-Line modeling of FOWT rotor aerodynamics to wind tunnel experiments. *J. Phys. Conf. Ser.* **2023**, *2626*, 012063. [CrossRef]
184. Arabgolarcheh, A.; Micallef, D.; Rezaeiha, A.; Benini, E. Modelling of two tandem floating offshore wind turbines using an actuator line model. *Renew. Energy* **2023**, *216*, 119067. [CrossRef]
185. Muzaferija, S. Computation of free surface flows using interface-tracking and interface-capturing methods. In *Nonlinear Water-Wave Interaction*; Computational Mechanics: Southampton, UK, 1998.
186. Xiu, D.; Karniadakis, G.E. The Wiener—Askey polynomial chaos for stochastic differential equations. *Siam. J. Sci. Comput.* **2002**, *24*, 619–644. [CrossRef]
187. Ghanem, R.G.; Spanos, P.D. *Stochastic Finite Elements: A Spectral Approach*; Courier Corporation: North Chelmsford, MA, USA, 2003.
188. Melchers, R.E.; Beck, A.T. *Structural Reliability Analysis and Prediction*; John wiley & sons: Hoboken, NJ, USA, 2018.
189. Rubinstein, R.Y.; Kroese, D.P. *Simulation and the Monte Carlo Method*; John Wiley & Sons: Hoboken, NJ, USA, 2016.
190. Huang, N.E.; Shen, Z.; Long, S.R. A new view of nonlinear water waves: The Hilbert spectrum. *Annu. Rev. Fluid Mech.* **1999**, *31*, 417–457. [CrossRef]
191. Sagaut, P. *Large Eddy Simulation for Incompressible Flows: An Introduction*; Springer Science & Business Media: Berlin/Heidelberg, Germany, 2005.
192. Cant, S. *SB Pope, Turbulent Flows*; Cambridge University Press: Cambridge, UK, 2000; 771p.
193. Li, Y.; Castro, A.M.; Sinokrot, T.; Prescott, W.; Carrica, P.M. Coupled multi-body dynamics and CFD for wind turbine simulation including explicit wind turbulence. *Renew. Energy* **2015**, *76*, 338–361. [CrossRef]
194. Yan, J.; Korobenko, A.; Deng, X.; Bazilevs, Y. Computational free-surface fluid–structure interaction with application to floating offshore wind turbines. *Comput. Fluids* **2016**, *141*, 155–174. [CrossRef]
195. Hirt, C.W.; Nichols, B.D. Volume of fluid (VOF) method for the dynamics of free boundaries. *J. Comput. Phys.* **1981**, *39*, 201–225. [CrossRef]
196. Vaz, G.; Jaouen, F.; Hoekstra, M. Free-surface viscous flow computations: Validation of URANS code FRESCO. In Proceedings of the International Conference on Offshore Mechanics and Arctic Engineering, Honolulu, HI, USA, 31 May–5 June 2009; Volume 43451, pp. 425–437.
197. Rapuc, S.; Crepier, P.; Jaouen, F.; Bunnik, T.; Regnier, P. Towards guidelines for consistent wave propagation in CFD simulations. In *Technology and Science for the Ships of the Future*; IOS Press: Amsterdam, The Netherlands, 2018; pp. 515–524.
198. Park, J.C.; Kim, M.H.; Miyata, H. Fully non-linear free-surface simulations by a 3D viscous numerical wave tank. *Int. J. Numer. Meth. Fl* **1999**, *29*, 685–703. [CrossRef]
199. Kim, H.; Lee, S.; Lee, S. Influence of blade-tower interaction in upwind-type horizontal axis wind turbines on aerodynamics. *J. Mech. Sci. Technol.* **2011**, *25*, 1351–1360. [CrossRef]
200. Tran, T.T.; Ryu, G.J.; Kim, Y.H.; Kim, D.H. CFD-based design load analysis of 5MW offshore wind turbine. *AIP Conf. Proc.* **2012**, *1493*, 533–545.
201. Kono, T.; Nebucho, S.; Kogaki, T.; Kiwata, T.; Kimura, S.; Komatsu, N. Numerical analysis of the effects of rotating wind turbine blades on the aerodynamic forces acting on tower. *Energies* **2017**, *10*, 121. [CrossRef]
202. Rockel, S.; Camp, E.; Schmidt, J.; Peinke, J.; Cal, R.B.; Hölling, M. Experimental study on influence of pitch motion on the wake of a floating wind turbine model. *Energies* **2014**, *7*, 1954–1985. [CrossRef]
203. Wen, B.; Tian, X.; Dong, X.; Peng, Z.; Zhang, W. Influences of surge motion on the power and thrust characteristics of an offshore floating wind turbine. *Energy* **2017**, *141*, 2054–2068. [CrossRef]
204. Jeon, M.; Lee, S.; Lee, S. Unsteady aerodynamics of offshore floating wind turbines in platform pitching motion using vortex lattice method. *Renew. Energy* **2014**, *65*, 207–212. [CrossRef]
205. Sivalingam, K.; Martin, S.; Singapore Wala, A.A. Numerical validation of floating offshore wind turbine scaled rotors for surge motion. *Energies* **2018**, *11*, 2578. [CrossRef]
206. Kyle, R.; Lee, Y.C.; Früh, W. Propeller and vortex ring state for floating offshore wind turbines during surge. *Renew. Energy* **2020**, *155*, 645–657. [CrossRef]
207. Tran, T.T.; Kim, D. A CFD study into the influence of unsteady aerodynamic interference on wind turbine surge motion. *Renew. Energy* **2016**, *90*, 204–228. [CrossRef]
208. Tran, T.T.; Kim, D.H. The aerodynamic interference effects of a floating offshore wind turbine experiencing platform pitching and yawing motions. *J. Mech. Sci. Technol.* **2015**, *29*, 549–561. [CrossRef]
209. Toan Tran, T.; Kim, D.; Hieu Nguyen, B. Aerodynamic interference effect of huge wind turbine blades with periodic surge motions using overset grid-based computational fluid dynamics approach. *J. Sol. Energy Eng.* **2015**, *137*, 061003. [CrossRef]
210. Tran, T.; Kim, D.; Song, J. Computational fluid dynamic analysis of a floating offshore wind turbine experiencing platform pitching motion. *Energies* **2014**, *7*, 5011–5026. [CrossRef]
211. Ren, N.; Li, Y.; Ou, J. Coupled wind-wave time domain analysis of floating offshore wind turbine based on Computational Fluid Dynamics method. *J. Renew. Sustain. Energy* **2014**, *6*, 023106. [CrossRef]
212. Tran, T.T.; Kim, D. Fully coupled aero-hydrodynamic analysis of a semi-submersible FOWT using a dynamic fluid body interaction approach. *Renew. Energy* **2016**, *92*, 244–261. [CrossRef]
213. Zhang, Y.; Kim, B. A fully coupled computational fluid dynamics method for analysis of semi-submersible floating offshore wind turbines under wind-wave excitation conditions based on OC5 data. *Appl. Sci.* **2018**, *8*, 2314. [CrossRef]

214. Quallen, S.; Xing, T. CFD simulation of a floating offshore wind turbine system using a variable-speed generator-torque controller. *Renew. Energy* **2016**, *97*, 230–242. [CrossRef]

215. Liu, Y.; Xiao, Q.; Incecik, A.; Peyrard, C.; Wan, D. Establishing a fully coupled CFD analysis tool for floating offshore wind turbines. *Renew. Energy* **2017**, *112*, 280–301. [CrossRef]

216. Zhou, Y.; Xiao, Q.; Peyrard, C.; Pan, G. Assessing focused wave applicability on a coupled aero-hydro-mooring FOWT system using CFD approach. *Ocean Eng.* **2021**, *240*, 109987. [CrossRef]

217. Feng, X.; Fang, J.; Lin, Y.; Chen, B.; Li, D.; Liu, H.; Gu, Y. Coupled aero-hydro-mooring dynamic analysis of floating offshore wind turbine under blade pitch motion. *Phys. Fluids* **2023**, *35*, 045131.

218. Cheng, P.; Huang, Y.; Wan, D. A numerical model for fully coupled aero-hydrodynamic analysis of floating offshore wind turbine. *Ocean Eng.* **2019**, *173*, 183–196. [CrossRef]

219. Huang, Y.; Wan, D. Investigation of interference effects between wind turbine and spar-type floating platform under combined wind-wave excitation. *Sustainability* **2019**, *12*, 246. [CrossRef]

220. Rodriguez, S.N.; Jaworski, J.W. Strongly-coupled aeroelastic free-vortex wake framework for floating offshore wind turbine rotors. Part 1: Numerical framework. *Renew. Energy* **2019**, *141*, 1127–1145.

221. Rodriguez, S.N.; Jaworski, J.W. Strongly-coupled aeroelastic free-vortex wake framework for floating offshore wind turbine rotors. Part 2: Application. *Renew. Energy* **2020**, *149*, 1018–1031. [CrossRef]

222. Liu, Y.; Xiao, Q. Development of a fully coupled aero-hydro-mooring-elastic tool for floating offshore wind turbines. *J. Hydrodyn.* **2019**, *31*, 21–33. [CrossRef]

223. Yu, Z.; Hu, Z.; Zheng, X.; Ma, Q.; Hao, H. Aeroelastic performance analysis of wind turbine in the wake with a new Elastic Actuator Line model. *Water* **2020**, *12*, 1233. [CrossRef]

224. Yu, Z.; Ma, Q.; Zheng, X.; Liao, K.; Sun, H.; Khayyer, A. A hybrid numerical model for simulating aero-elastic-hydro-mooring-wake dynamic responses of floating offshore wind turbine. *Ocean Eng.* **2023**, *268*, 113050. [CrossRef]

225. Campaña-Alonso, G.; Martin-San-Román, R.; Méndez-López, B.; Benito-Cia, P.; Azcona-Armendáriz, J. OF 2: Coupling OpenFAST and OpenFOAM for high fidelity aero-hydro-servo-elastic FOWT simulations. *Wind Energy Sci. Discuss.* **2023**, *8*, 1597–1611. [CrossRef]

226. Calderer, A.; Guo, X.; Shen, L.; Sotiropoulos, F. Coupled fluid-structure interaction simulation of floating offshore wind turbines and waves: A large eddy simulation approach. *J. Phys. Conf. Ser.* **2014**, *524*, 012091. [CrossRef]

227. Xu, S.; Zhuang, T.; Zhao, W.; Wan, D. Numerical investigation of aerodynamic responses and wake characteristics of a floating offshore wind turbine under atmospheric boundary layer inflows. *Ocean Eng.* **2023**, *279*, 114527. [CrossRef]

228. Lamei, A.; Hayatdavoodi, M.; Wong, C.; Tang, B. On Motion and Hydroelastic Analysis of a Floating OffshoreWind Turbine. In Proceedings of the International Conference on Offshore Mechanics and Arctic Engineering, Scotland, UK, 9–14 June 2019; Volume 58899, p. V010T09A070.

229. Zhang, Y.; Hu, Z. An aero-hydro coupled method for investigating ship collision against a floating offshore wind turbine. *Mar. Struct.* **2022**, *83*, 103177. [CrossRef]

230. Lienard, C.; Boisard, R.; Daudin, C. Aerodynamic behavior of a floating offshore wind turbine. *AIAA J.* **2020**, *58*, 3835–3847. [CrossRef]

231. Santo, G.; Peeters, M.; Van Paepegem, W.; Degroote, J. Fluid–structure interaction simulations of a wind gust impacting on the blades of a large horizontal axis wind turbine. *Energies* **2020**, *13*, 509. [CrossRef]

232. Sayed, M.; Lutz, T.; Krämer, E.; Shayegan, S.; Wüchner, R. Aeroelastic analysis of 10 MW wind turbine using CFD–CSD explicit FSI-coupling approach. *J. Fluid. Struct.* **2019**, *87*, 354–377. [CrossRef]

233. Mann, J. The spatial structure of neutral atmospheric surface-layer turbulence. *J. Fluid. Mech.* **1994**, *273*, 141–168. [CrossRef]

234. Kaimal, J.C.; Wyngaard, J.; Izumi, Y.; Coté, O.R. Spectral characteristics of surface-layer turbulence. *Q. J. Roy Meteor. Soc.* **1972**, *98*, 563–589.

235. Li, L.; Liu, Y.; Yuan, Z.; Gao, Y. Wind field effect on the power generation and aerodynamic performance of offshore floating wind turbines. *Energy* **2018**, *157*, 379–390. [CrossRef]

236. Doubrawa, P.; Churchfield, M.J.; Godvik, M.; Sirnivas, S. Load response of a floating wind turbine to turbulent atmospheric flow. *Appl. Energy* **2019**, *242*, 1588–1599. [CrossRef]

237. Nybø, A.; Nielsen, F.G.; Reuder, J.; Churchfield, M.J.; Godvik, M. Evaluation of different wind fields for the investigation of the dynamic response of offshore wind turbines. *Wind Energy* **2020**, *23*, 1810–1830. [CrossRef]

238. Hsieh, A.S.; Brown, K.A.; DeVelder, N.B.; Herges, T.G.; Knaus, R.C.; Sakievich, P.J.; Cheung, L.C.; Houchens, B.C.; Blaylock, M.L.; Maniaci, D.C. High-fidelity wind farm simulation methodology with experimental validation. *J. Wind Eng. Ind. Aerod.* **2021**, *218*, 104754. [CrossRef]

239. Munters, W.; Meyers, J. Dynamic strategies for yaw and induction control of wind farms based on large-eddy simulation and optimization. *Energies* **2018**, *11*, 177. [CrossRef]

240. Richards, P.J.; Hoxey, R.P. Appropriate boundary conditions for computational wind engineering models using the k-ϵ turbulence model. *J. Wind Eng. Ind. Aerod.* **1993**, *46*, 145–153. [CrossRef]

241. Richards, P.J.; Norris, S.E. Appropriate boundary conditions for computational wind engineering models revisited. *J. Wind Eng. Ind. Aerod.* **2011**, *99*, 257–266. [CrossRef]

242. Liu, Y.; Chen, D.; Li, S. The artificial generation of the equilibrium marine atmospheric boundary layer for the CFD simulation of offshore wind turbines. *J. Wind Eng. Ind. Aerod.* **2018**, *183*, 44–54. [CrossRef]

243. Blocken, B.; Stathopoulos, T.; Carmeliet, J. CFD simulation of the atmospheric boundary layer: Wall function problems. *Atmos. Environ.* **2007**, *41*, 238–252. [CrossRef]

244. Yang, Y.; Xie, Z.; Gu, M. Consistent inflow boundary conditions for modelling the neutral equilibrium atmospheric boundary layer for the SST k-ω model. *Wind Struct.* **2017**, *24*, 465–480. [CrossRef]

245. Zhang, L.; Li, Y.; Xu, W.; Gao, Z.; Fang, L.; Li, R.; Ding, B.; Zhao, B.; Leng, J.; He, F. Systematic analysis of performance and cost of two floating offshore wind turbines with significant interactions. *Appl. Energy* **2022**, *321*, 119341. [CrossRef]

246. Wang, L.; Robertson, A.; Kim, J.; Jang, H.; Shen, Z.; Koop, A.; Bunnik, T.; Yu, K. Validation of CFD simulations of the moored DeepCwind offshore wind semisubmersible in irregular waves. *Ocean Eng.* **2022**, *260*, 112028. [CrossRef]

247. Zhang, Y.; Xu, H.; Law, Y.; Santo, H.; Magee, A. Hydrodynamic analysis and validation of the floating DeepCwind semi-submersible under 3-h irregular wave with the HOS and CFD coupling method. *Ocean Eng.* **2023**, *287*, 115701. [CrossRef]